



4-Aryl-4-oxo-*N*-phenyl-2-aminybutyramides as acetyl- and butyrylcholinesterase inhibitors. Preparation, anticholinesterase activity, docking study, and 3D structure–activity relationship based on molecular interaction fields

Maja D. Vitorović-Todorović^{a,b,*}, Ivan O. Juranić^b, Ljuba M. Mandić^b, Branko J. Drakulić^c

^a Military-Technical Institute, Ratka Resanovića 1, Belgrade, Serbia

^b Faculty of Chemistry, University of Belgrade, Studentski Trg 12-16, Belgrade, Serbia

^c Department of Chemistry-ICHM, University of Belgrade, Njegoševa 12, Belgrade, Serbia

ARTICLE INFO

Article history:

Received 1 July 2009

Revised 16 November 2009

Accepted 15 December 2009

Available online 22 December 2009

Keywords:

4-Aryl-4-oxo-*N*-phenyl-2-aminybutyramides

Anticholinesterase activity

Mixed-type reversible inhibitors

Alignment-independent 3D QSAR

Docking study

ABSTRACT

Synthesis and anticholinesterase activity of 4-aryl-4-oxo-*N*-phenyl-2-aminybutyramides, novel class of reversible, moderately potent cholinesterase inhibitors, are reported. Simple substituent variation on aroyl moiety changes anti-AChE activity for two orders of magnitude; also substitution and type of hetero(alicycle) in position 2 of butanoic moiety govern AChE/BChE selectivity. The most potent compounds showed mixed-type inhibition, indicating their binding to free enzyme and enzyme–substrate complex. Alignment-independent 3D QSAR study on reported compounds, and compounds having similar potencies obtained from the literature, confirmed that alkyl substitution on aroyl moiety of molecules is requisite for inhibition activity. The presence of hydrophobic moiety at close distance from hydrogen bond acceptor has favorable influence on inhibition potency. Docking studies show that compounds probably bind in the middle of the AChE active site gorge, but are buried deeper inside BChE active site gorge, as a consequence of larger BChE gorge void.

© 2009 Elsevier Ltd. All rights reserved.

1. Introduction

Alzheimer's disease (AD) accounts for 50% cases of dementia in elderly people, is a complex, progressive neurodegenerative disorder, followed by decrease of cognitive functions such as altered ability of memory and learning and behavioral disturbances. The main pathological hallmarks of the disease comprise: extracellular formation of senile amyloid- β -peptide (A β) plaques, the loss of cholinergic neurons from basal forebrain and thereby decreased levels of neurotransmitter acetylcholine (ACh) and enzymes involved in its synthesis and hydrolysis: acetylcholinesterase (ChAT) and acetylcholinesterase (AChE). Among different strategies investigated to improve cholinergic neurotransmission, the reduction of ACh hydrolysis by AChE inhibitors is up to date the prevalent effective AD symptomatic treatment.¹

AChE contains 20 Å deep and narrow gorge, in which five regions that are involved in the substrate, the irreversible and reversible inhibitor binding (*human* and *electric eel* AChE numbering), can be distinguished: (1) catalytic triad residues: Ser 203, His 447, and Glu 334,² at the bottom of the gorge, which directly participate in catalytic cycle, by charge relay mechanism, as in other serine esterases,^{3,4} (2) oxyanion hole represents the arrangement of hydrogen

bond donors which stabilize the transient tetrahedral enzyme–substrate complex by accommodation of negatively charged carbonyl oxygen. This region inside of active center is formed by peptide –NH– groups of amino acid residues Gly 121, Gly 122, and Ala 204,^{5,6} (3) the 'anionic site' (AS), where Trp 86 is situated. This residue is conserved in all cholinesterases and it is involved in orientation and stabilization of trimethylammonium group of ACh, by forming cation- π interactions,^{7–10} (4) acyl pocket comprises two phenylalanine residues in positions 295 and 297, which interacts with the substrate acyl group. They form the clamps around acetyl methyl group of acetylcholine, and decrease its degrees of freedom,¹¹ (5) peripheral anionic site (PAS)^{12–14} comprises residues which are located on the rim of the active site gorge, Tyr 72, Tyr 124, Trp 286, and Asp 74. Possible binding sites for the reversible inhibitors comprise AS and PAS. The so-called dimeric (dual) inhibitors bind to both sites.

Up to now, AChE inhibition represented the pure palliative treatment for AD. However in the past decade, another, non-catalytic roles of the enzyme have been established. It was demonstrated that AChE has a key role in the acceleration of A β -peptide deposition and promoting the formation of A β -plaques.¹⁵ It is proved that AChE inhibitors, which bind to PAS, could inhibit such processes.¹⁶ Today, the importance of AChE's sister enzyme, butyrylcholinesterase (BChE), also rises as a pharmacological target for AD therapy. It was found that BChE is capable to compensate AChE

* Corresponding author. Tel.: +381 11 3336738; fax: +381 11 2636061.

E-mail address: mvitod@chem.bg.ac.rs (M.D. Vitorović-Todorović).

catalytic functions in synaptic cleft^{17,18} and that its activity significantly increases, for 30–60%, during time course in AD.^{19,20} Of four FDA approved AChE inhibitors, only donepezil binds simultaneously to active and peripheral anionic sites, but the inhibition of A β aggregation is modest.¹⁵ Actually, an inhibitor of AChE and BChE that strongly interact with PAS, or with both PAS and active site (like dimeric inhibitors), and that exhibit inhibitory effect against AChE induced A β aggregation, is needed.

Recently, it was shown that some α,β -unsaturated compounds exhibit good inhibition potency toward both AChE and BChE. Those are chalcones²¹ (**I**), which show affinities in micromolar range and *m*- and *p*-aminobenzoic acid maleamides (**II**) and maleimides (**III**) (Fig. 1), which are potent nanomolar inhibitors.^{22–25} Some of these derivatives act as irreversible inhibitors, probably because of Michael-type addition of nucleophilic groups present in the active site gorge. From pharmacokinetic point of view, the presence of Michael acceptor in drug structure could be considered as disadvantage, because of high reactivity, instability in physiological conditions, and low selectivity. However, saturated analogues of *m*-aminobenzoic acid maleamides show even higher inhibition potency, compared to unsaturated ones, indicating that α,β -unsaturation is not necessary for anti-AChE activity.²² Therefore, the presence of activated double bond can be used for further functionalization, by the addition of suitably chosen nucleophiles that bear moieties which could favorably interact with amino acid residues inside AChE and BChE active site gorge.

In continuation of our work on aroylacrylic acids and their phenylamides, we decided to use the reactivity of ketovinyl moiety toward common nucleophiles and to combine aroylacrylic acid anilides (**IV**) with amines as nucleophiles, to obtain the corresponding Michael adducts as enantiomeric mixtures.

Aroylacrylic acid anilides were chosen because they combine amidic and α,β -unsaturated carbonyl moiety of aminobenzoic acid maleamides, and ring A of chalcones.

As nucleophiles common scaffold of AChE inhibitors, piperidine, morpholine, and imidazole were chosen.^{26–30} Also 1,8-diaminooctane was used to obtain dimeric inhibitors. Inhibition potency of the obtained compounds (**1–26**, Fig. 2) toward *Electric Eel* AChE and horse serum BChE was tested by spectrophotometric method of Ellman et al.,³¹ using acetyl- and butyrylthiocholine iodide as substrates and tacrine as a reference standard.

2. Results and discussion

2.1. Chemistry

Synthetic pathway to **1–26** is given in Scheme 1. Friedel–Crafts acylation of the commercially available substituted benzenes (**A**) with maleic acid anhydride (**B**) yields aroylacrylic acids (**C**).³² Sub-

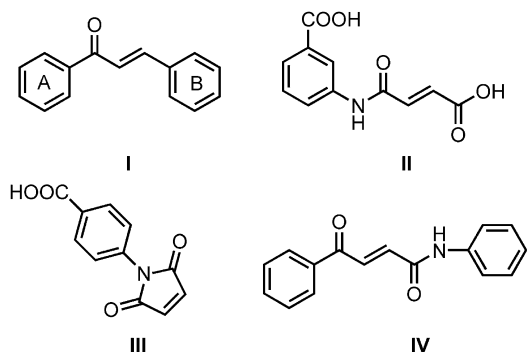


Figure 1. Chalcones (**I**), *p*- and *m*-aminobenzoic acid amides (**II**), and imides (**III**), aroylacrylic acid anilides (**IV**).

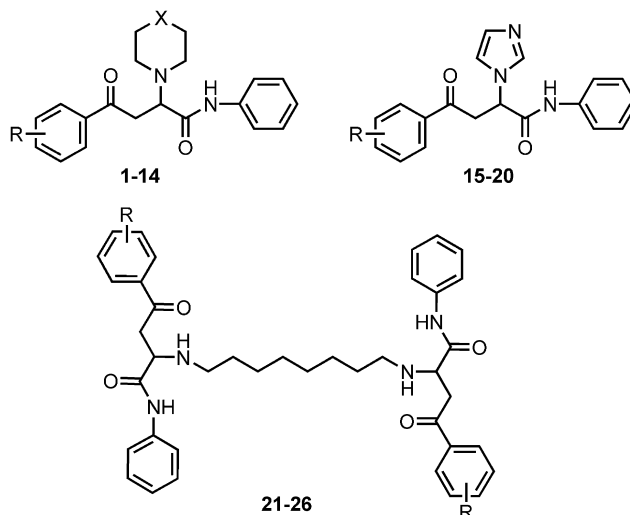


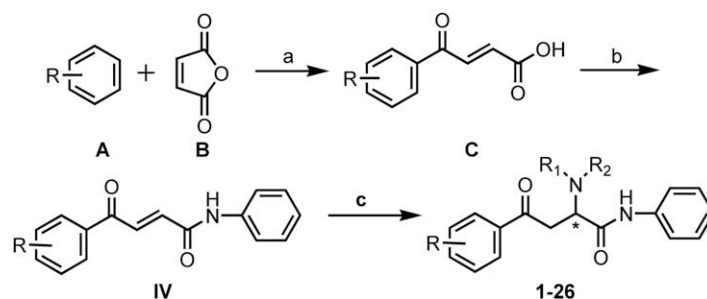
Figure 2. Novel 4-aryl-4-oxo-N-phenyl-2-aminylbutyramides, X = $-\text{CH}_2-$ (**1–7**) or $-\text{O}-$ (**8–14**), and dimeric analogues (**21–26**).

sequently, the acids were converted to acid chlorides in dry THF by phosphorous-oxychloride, then in situ reacted with equimolar amounts of aniline to give the corresponding anilides (**IV**).³³ Michael type addition of the corresponding amine (piperidine, morpholine, imidazole, or 1,8-diaminooctane) to aroylacrylic acid anilide double bond, proceeded smoothly to give target compounds **1–26**. Actually, Michael addition of piperazine and diisopropylamine has also been tried. However, the expected diisopropylamine adduct has not been obtained, probably because of steric reasons. Mixture of **IV** and 2–10-fold excess of piperazine always yielded dimeric products, insoluble in common solvents. Target compounds were characterized by ¹H and ¹³C NMR spectroscopy and by LC–HRMS (ESI).

2.2. Biological activity, QSAR, and molecular modeling

Inhibition potency of compounds toward AChE and BChE, expressed as IC₅₀ values is shown in Table 1. The inhibition potency of dimeric analogues **21–26** toward both enzymes was not determined, due to their insolubility in assay conditions. Considering the effects of piperidine derivatives **1–7** on AChE activity, voluminous alkyl substituents, 4-*i*-Pr, 2,4-di-*i*-Pr, and β -tetalinoyl, in **5–7**, decrease IC₅₀ values for at least two orders of magnitude, in respect to unsubstituted derivative **1**, which does not show any inhibition of AChE activity at the concentration of 100 μM . Similar effects were observed for imidazolo derivatives (**15–20**), except for insoluble **16**. Derivatives **18–20**, which bear voluminous alkyl groups, exert higher potency. Due to a very low solubility of morpholino derivatives (**8–14**) in water media, determination of IC₅₀ values was not possible, only a percent of inhibition for **11** at the highest concentration tested is reported. Three analogues do not show any inhibition activity at 100 μM . It is clear that the presence of morpholino oxygen instead of piperidine methylene group has a negative influence on inhibition potency. The 4-MeO derivative (**11**) shows 38.7% inhibition of enzyme activity at inhibitor concentration of 100 μM , and 4-*i*-Pr analogue (**12**) does not show any inhibition at the same concentration. Consequently, unlike piperidino and imidazolo derivatives, the presence of voluminous alkyl groups does not contribute to the inhibition potency of morpholino derivatives. The most potent of all analogues toward AChE is **19**.

Considering the effects of **1–26** on BChE activity, only one or two compounds within each subgroup are active (Table 1). Percent of enzyme inhibition at the highest tested inhibitor concentration



Scheme 1. Synthesis of **1–26**. Reagents: (a) AlCl_3 ; (b) POCl_3 , aniline/THF; (c) NR_2 (piperidine, imidazole, morpholine, octane-1,8-diamine) in $\text{CHCl}_3/\text{C}_6\text{H}_6$.

Table 1
IC₅₀ values of the synthesized Michael adducts (**1–20**) toward AChE and BChE

Compound	R	IC ₅₀ ± SE (μM)	
		AChE	BChE
1	H–	>100	34.81% @ 100 ^a
2	2,5-Di-Me–	>10	17.18 ± 0.12
3	4-Cl–	Ins ^b	Ins
4	4-MeO–	>10	>40
5	4- <i>i</i> -Pr–	3.47 ± 0.04	7.06 ± 0.04
6	2,4-di- <i>i</i> -Pr–	4.86 ± 0.03	39.93% @ 15
7	β-Tetralinoyl–	5.64 ± 0.02	21.50% @ 15
8	H–	>100	21.55% @ 100
9	2,5-Di-Me–	>100	34.12 ± 0.16
10	4-Cl–	Ins	Ins
11	4-MeO–	38.7% @ 100	>100
12	4- <i>i</i> -Pr–	>100	27.22% @ 40
13	2,4-Di- <i>i</i> -Pr–	>10	2.48 ± 0.01
14	β-Tetralinoyl–	>30	13.00% @ 40
15	2,5-Di-Me–	27.86 ± 1.05	42.00% @ 70
16	4-Cl–	Ins	Ins
17	4-MeO–	7.85 ± 0.03	30.41 ± 0.56
18	4- <i>i</i> -Pr–	8.22 ± 0.04	10.00% @ 30
19	2,4-Di- <i>i</i> -Pr–	1.55 ± 0.01	>20
20	β-Tetralinoyl–	6.34 ± 0.01	17.00% @ 40
Tacrine		42.95 ± 0.01 nM	6.95 ± 0.01 nM

^a Percent of inhibition at given concentration.

^b Insoluble in methanol.

shows that piperidino and morpholino analogues are more potent than imidazolo ones. Alkyl substituted piperidino derivatives exert higher inhibition potency, compared to unsubstituted analogue **1** (34.81% of enzyme inhibition at 100 μM). Two of morpholino analogues, **9** and **13**, are active. Unsubstituted morpholino derivative (**8**) does not show any inhibition effect, and 4-MeO derivative (**11**) shows very low inhibition at the highest concentration tested (100 μM). Thus, alkyl substitution of morpholino analogues has favorable influence on inhibition potency toward BChE. Because of lower inhibition potency of imidazolo analogues toward BChE compared to AChE, and their low solubility in assay conditions, only the potency of 4-MeO analogue (**17**) was determined.

From Table 1, it is clear that generally piperidino and imidazolo derivatives are more active toward AChE. However three morpholino derivatives do not show any inhibition potency of AChE activity up to 100 μM, but five of them have some activity toward BChE in concentrations lower than 100 μM. So, the type of heterocyclic substitution at position 2 of butanoic moiety not only has impact on AChE activity, but also results in AChE/BChE selectivity.

Subsequently, the spectrophotometric method of Ellman was used to determine the type of inhibition and the K_i values of two most active compounds, **19** and **13**, toward AChE and BChE, respectively. Both compounds exhibited mixed type of inhibition toward the corresponding enzymes. This behavior was indicated by intersection of double reciprocal lines in the upper left quadrant (Lineweaver–Burk plot) represented in Figures 3 and 4 for **19** and

13, respectively. Generally, this type of inhibition is the result of combination of partially competitive and non-competitive inhibitions, indicating binding to free enzyme and to enzyme–substrate complex, that is, a possible binding to site remote from the active site. The obtained K_i 's are 4.66 μM for **19** (AChE) and 3.18 μM for **13** (BChE).

To gain a deeper insight into pharmacophoric pattern that governs differences in the potency of **1–20**, the literature was mined for compounds that exert activity toward *Electric Eel* AChE in similar concentrations range. The AChE has anionic and peripheral binding sites, and dual inhibitors fit simultaneously to both sites. Such molecules usually comprise two heterocyclic moieties connected with the linker of different lengths, and consequently have large volumes. To preclude consideration of compounds that could act as dual inhibitors, within the set obtained by the literature search, only those having volume less than 10% larger of the most voluminous **6** were considered for further modeling study.

Totally 38 compounds were collected, including secolycorines (**1–1** to **1–8**),³⁴ 1-[bis(4-fluorophenyl)-methyl]piperazines (**2–9** to **2–11**),²⁸ litebammine derivatives (**3–12** to **3–21**),³⁵ imidazolyl-isoxazolines (**4–22** to **4–27**),³⁶ 3-aryl-*N*-methyl-tetrahydropyridine derivatives (**5–28** and **5–30**),³⁷ and **5–7**, **15**, **17–20** (Scheme 2); spanning range of potencies 0.8–240 μM (~2.5 log(1/(IC₅₀)) units).

All compounds were submitted to Pentacle, and for model building HBD (N1), HBA (O), and hydrophobic (DRY) probe were used. The obtained model has good statistics and predictivity (Tables 2 and 3). Partial least square (PLS) coefficient plot obtained

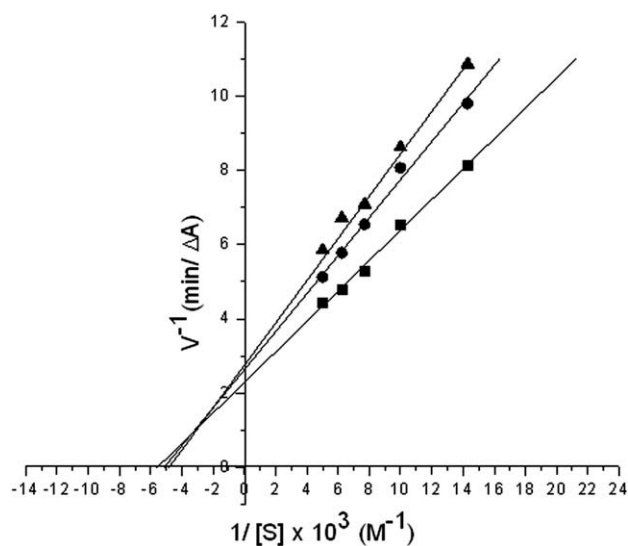


Figure 3. Lineweaver–Burk plot of AChE (0.02 U) with substrate acetylthiocholine, in the absence or presence of different concentrations of **19**. (■) No inhibitor; (●) 1.0 μM; (▲) 1.5 μM.

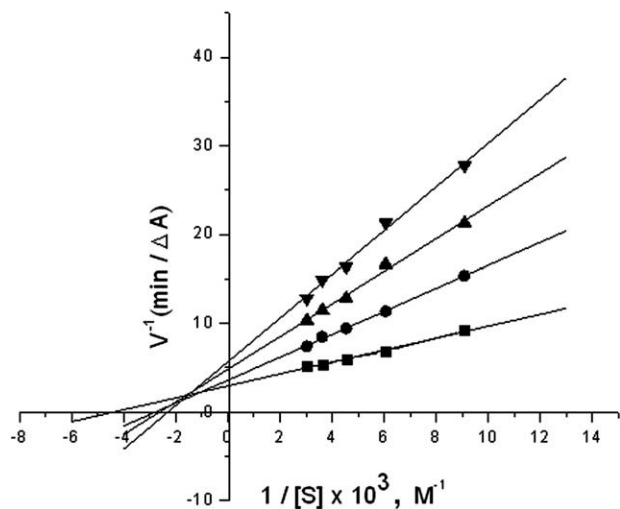


Figure 4. Lineweaver–Burk plot of BChE (0.02 U) with substrate acetylthiocholine, in the absence or presence of different concentrations of **13**. (■) No inhibitor; (●) 1.0 μM ; (▲) 2.0 μM ; (▼) 3.0 μM .

with 5 latent variables is given in Figure 5. Variables expressed for particular compound are given in Table S1 in Supplementary. Experimental versus predicted $\log(1/(\text{IC}_{50}))$ values are given in Table 4. Full analysis of the model is out of the scope of this article, therefore the main observations that give significant information on pharmacophoric pattern of molecules will be discussed in the following lines. Bulk of variables having high impact on the model, positively or negatively correlated with activity, are expressed for the majority of **5–7**, **15**, **17–20** (see Table S1 in Supplementary). This means that the reported compounds share spatial arrangement of pharmacophoric points (including their interaction energies with the GRID probes used) with structurally very diverse (dissimilar) compounds reported in the literature, having potencies toward *E. Eel* AChE in a comparable range of concentrations. For

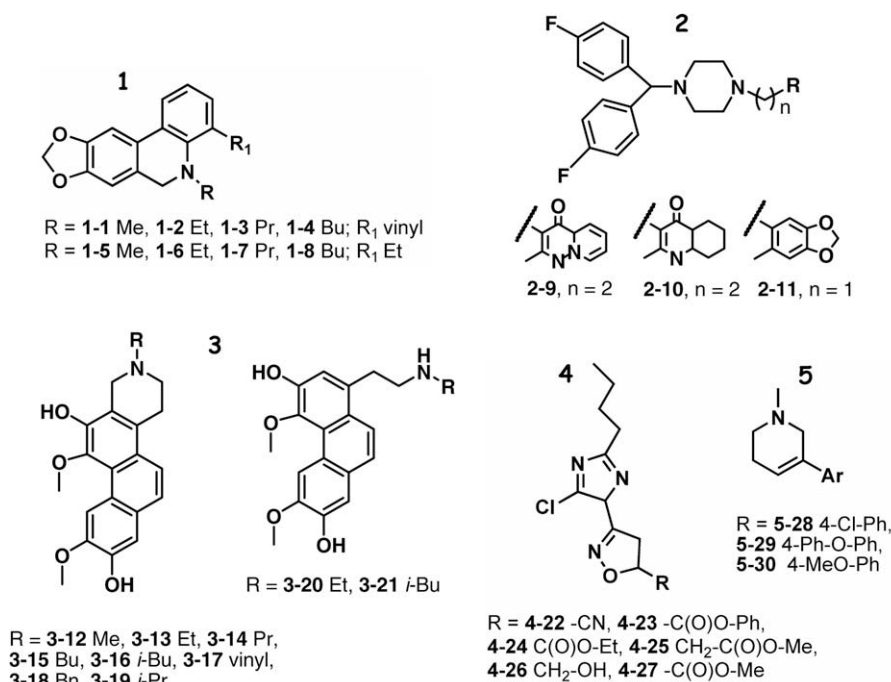
Table 2
PCA model

Comp.	SSx	SSx _{acc}	VarX	VarX _{acc}
1	53.95	53.95	52.55	52.55
2	17	70.95	16.58	69.13
3	6.19	77.14	5.80	74.93
4	4.46	81.60	4.22	79.16
5	3.26	84.86	3.11	82.27

Comp.—number of components; SSX—percentage of the X sum of squares; SSX_{acc}—accumulative percentage of the X sum of squares; VarX—percentage of the X variance; VarX_{acc}—accumulative percentage of the X variance.

example, variables DRY-DRY 41, 42 that describe the presence of two hydrophobic moieties in molecules on 13.12–13.76 Å, having IE with DRY probe of ~ -1.4 kcal/mol (Fig. S1 in Supplementary), are expressed for the majority of compounds. Important variables that offer data on differences among molecules are commented in more detail. Variable DRY-N1 260 is expressed only for **2–11**, one of the most potent of the studied molecules in the set, as well as for **5**, **6**, and **19**, the most potent among the prepared compounds. This variable recognizes spatial proximity of HBA (~ -6.2 kcal/mol) and hydrophobic region of molecules (~ -1.26 kcal/mol), Figure 6. Variable O-N1 359, negatively correlated with the potency of compounds, gives almost sharp cut-off between more and less active compounds within the studied set. This variable is expressed for the vast majority of compounds having potencies on or below 2.1 $p(\text{IC}_{50})$. Additionally, variable is expressed for the one of less potent **17** (Fig. S2 in Supplementary). It is obvious that the presence of HBA (N1 probe IE ~ -4.00 kcal/mol) and HBD (O probe IE ~ -4.75 kcal/mol) in molecules, on 12.48–12.80 Å has unfavorable influence on the potency of compounds. Matrix-like representation of compound corelograms (Pentacle heat maps), allow clear observation of this difference (Fig. S3 in Supplementary).

Next, we try to find variables that differentiate **5–7**, **15**, **17–20** in respect to potency. Variable DRY-N1 302 (nodes distance 14.72–15.04 Å), positively correlated with potency, even not having high impact on whole model, nicely differentiate less potent **15** from the rest of the compounds. This variable is positioned be-

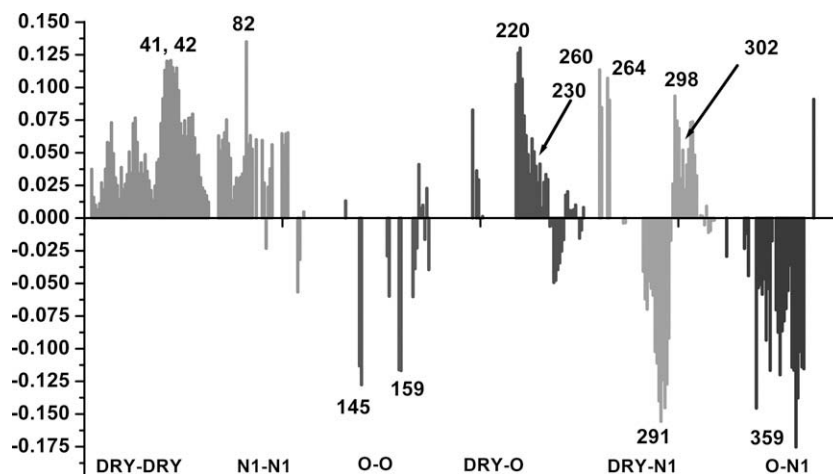


Scheme 2. Structural formulae of **1–1** to **5–30**.

Table 3
PLS model

Comp.	SSX	SSX _{acc}	SDEC	SDEP	R ²	R _{acc} ²	RG-Q _{acc} ²	LTO-Q _{acc} ²	LOO-Q _{acc} ²
1	53.16	53.16	0.52	0.56	0.24	0.24	0.10	0.13	0.13
2	7.66	60.82	0.34	0.51	0.42	0.66	0.25	0.31	0.32
3	13.26	74.08	0.28	0.46	0.12	0.78	0.40	0.44	0.45
4	3.36	77.44	0.20	0.41	0.10	0.89	0.51	0.60	0.61
5	4.34	81.78	0.18	0.40	0.02	0.91	0.54	0.60	0.61

Comp.—number of components; SSX—percentage of the X sum of squares; SSX_{acc}—accumulative percentage of the X sum of squares; SDEPs—standard deviation error of the predictions; R²—coefficient of determination; R_{acc}²—accumulative coefficient of determination; Q_{acc}²—accumulative squared predictive correlation coefficient (RGs—random groups; LTO—leave two out; LOO—leave one out).

**Figure 5.** PLS coefficient plot for the reported model, obtained with 5 LV.

tween aroyl–alkyl substituents (DRY) and imidazolo or piperidino N (N1) for **5**, **6**, **18–20**, (Fig. 7) but not for the less potent **15**. Additionally, variable DRY-O 230 (12.16–12.46 Å), which connects extended hydrophobic moieties on aryl ring and amido NH, is expressed only for **5–7** and **18–20** (Fig. 8), but not for the less potent **15** and **17**. It should be noted that not only mere lipophilicity of aroyl fragment, but also position of substituents differentiates **5–7**, **15**, **17–20** in respect to potency. In Figure S4 in Supplementary log(1/(IC₅₀)) versus GRID DRY probe volume obtained on –0.55 kcal/mol is shown. The most potent **19** and the less potent **15** significantly deviate from correlation, which is obvious for the rest of the compounds. Even **15** and **19** have similar isovolumes of the DRY probe on chosen IE, their potencies are significantly different. Observing the DRY isovolumes around molecules, it may be concluded that different substitution patterns of aroyl moiety influence their potencies.

In summary, reported analysis revealed few important points, which will be guidance for designing of novel compounds. First, the presence of aroyl phenyl and amidophenyl rings of molecules fits to the two hydrophobic areas separated by ~13.5 Å (variable DRY-DRY 41) in the majority of, structurally diverse, compounds in the set. Second, alkyl substitution on aroyl moieties of molecules is requisite, and most favorable positions are 2 and 4. Variable DRY-N1 302 shows that suitably chosen extended hydrophobic moiety on aroyl phenyl ring can fine-tune the potency of compounds toward *E. Eel* AChE, allowing prerequisite distance between HBA and hydrophobic moiety. On the other hand, it is clear from Table 1 that the introduction of substituents on phenyl ring turns inactive compounds (IC₅₀ >100 μM) to moderately potent ones, consequently change of potency for ~2 orders of magnitude was obtained. Third, the need for specific spatial arrangement of HBA and hydrophobic moiety of molecules on close distance (1.28–

1.60 Å), given by variable DRY-N1 260,[†] which can be found for three most potent compounds (**5**, **6**, and **19**), as well as for the one of the most potent compounds within the studied set. For **5–7**, **15**, **17–20**, this feature is governed by nature and position of phenyl substituents on aroyl moiety, as well as by the nature of hetero(ali)cycle on the position 2 of butanoic moiety, which result in geometry that allows favorable spatial arrangement of pharmacophoric points (for the description of conformers generation used in the model see Section 4). Fourth, and this holds for the whole studied set, the presence of HBA and HBD on spatial distance of ~12.5 Å yields less potent compounds, therefore for novel congeners alkoxy or hydroxy substituents on aroyl ring should be avoided.

To investigate possible ligand–AChE interactions, docking studies were performed to generate binding model for the most active piperidino (**5**) and imidazolo (**19**) derivatives toward AChE. Both enantiomers of **5** and **19** were docked to mAChE (*Mus Musculus*, PDB code 2HA2). This AChE crystal structure was chosen because it has the same conserved amino acid residues as the only available EeAChE crystal structure has (PDB code 1C2B), but with considerably better resolution. Docking studies were performed using the latest version of AUTODOCK 4.0.1 package,³⁸ which allows flexibility of small ligands and of user defined amino acid residues in the receptor. As flexible, three tyrosine residues were chosen (72, 337, and 341). Crystallographic data¹⁴ and molecular dynamic simulations³⁹ revealed considerable mobility of these residues. Tyr 337 is located midway in the gorge and its motion could enlarge the volume of active site gorge. Homologous residue Phe 330 in TcAChE was also found to be flexible.⁴⁰ Side-chain motion of Tyr 341 might significantly enlarge the gorge mouth and facilitate

[†] For clarity: DRY probe is complementary with hydrophobic moieties of molecules, while N1 (HBD) probe is complementary with HBA moieties of molecules.

Table 4

Experimental versus predicted $\log(1/(IC_{50}))$ as obtained by the Pentacle model described in the text

Comp.	$\log(1/(IC_{50}))$ Exp.	$\log(1/(IC_{50}))$ Pred.
5	2.460	2.384
6	2.313	2.361
7	2.249	2.305
15	1.555	1.864
17	2.105	2.081
18	2.085	2.217
19	2.810	2.454
20	2.198	2.277
1-1	2.539	2.131
1-2	2.078	2.145
1-3	1.975	2.296
1-4	2.575	2.250
1-5	2.523	2.208
1-6	2.055	2.182
1-7	2.001	2.159
1-8	2.264	2.237
2-9	2.672	2.620
2-10	2.917	2.842
2-11	2.945	3.106
3-12	1.658	1.618
3-13	1.840	1.732
3-14	2.142	2.091
3-15	2.108	2.061
3-16	2.186	2.052
3-17	1.801	1.980
3-18	1.972	1.843
3-19	2.167	2.127
3-20	1.565	1.393
3-21	1.208	1.480
4-22	2.699	2.535
4-23	1.142	1.334
4-24	1.157	1.057
4-25	0.795	0.817
4-26	1.678	1.658
4-27	0.618	0.770
5-28	3.094	3.055
5-29	2.909	3.163
5-30	2.909	3.083

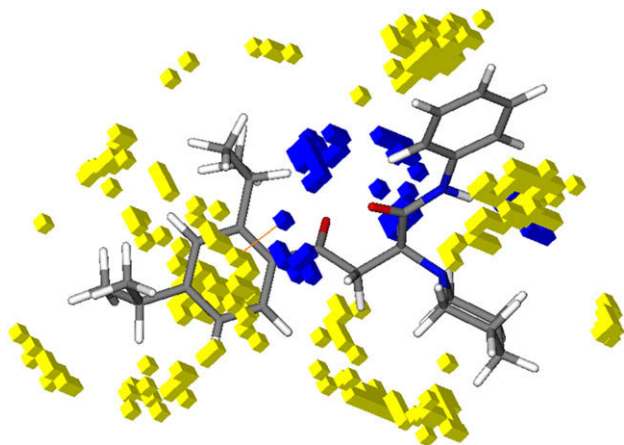


Figure 6. Variable DRY-N1 260 (1.28–1.60 Å) recognizes proximity of HBA and hydrophobic region of molecules. Compound 5, yellow boxes DRY probe field, blue boxes N1 probe field.

the ligand access to catalytic site. The lowest energy cluster returned by AUTODOCK for each enantiomer of **5** and **19** was used for further analysis. Best docking solutions for all docked derivatives revealed that the positions of flexible tyrosine residues were not significantly changed in respect to their positions in the free enzyme. Major change was the movement of Tyr 337 side chain toward indole ring of Trp 86, and possible formation of hydrogen

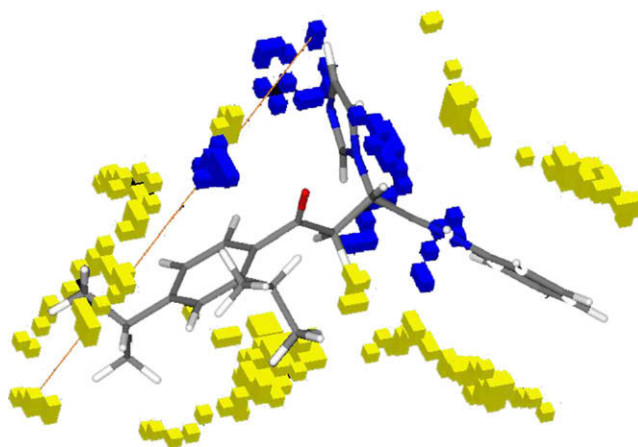


Figure 7. Variable DRY-N1 302 (14.72–15.04 Å) shows prerequisite distance between HBA and hydrophobic moiety. Compound 19, yellow boxes DRY probe field, blue boxes N1 probe field.

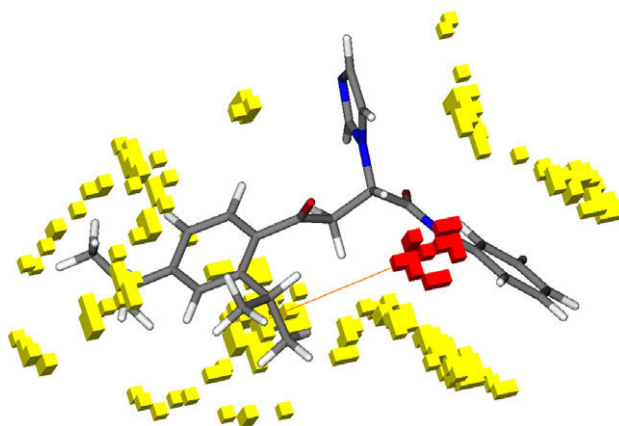


Figure 8. Variable DRY-O 230 (12.16–12.46 Å), distance between HBD and hydrophobic moiety. Compound 19, yellow boxes DRY probe field, red boxes O probe field.

bond between Tyr 337 –OH and indole –NH– group. The same has been observed in docking studies with HuAChE.⁴¹ Docking studies show that **19** (*R*) binds in the middle of AChE active site gorge, Figure 9a. Phenylamido group is directed toward Trp 286 and forms hydrophobic contacts with its side chain, with minimal distance of 3.74 Å. Imidazole ring is found near Phe 297 aromatic ring (minimal distance 3.76 Å), its nitrogen atom forms hydrogen bond with Phe 295 backbone –NH– group. Aroyl moiety is directed toward the bottom of the gorge. Interestingly, orientation of **19** (*S*) inside AChE active site gorge is reversed (Fig. 9b). Aroyl group is directed toward the entrance of the gorge. Its phenyl ring forms close hydrophobic contact to Phe 338 (4.64 Å) and Tyr 341 (3.82 Å) aromatic side chains. Imidazole ring is found near Ser 125 side chain (3.86 Å) and near backbone –NH– group of Asp 74 (3.53 Å). Amido carbonyl group forms hydrogen bond to Ser 125 –OH group (2.04 Å). Phenylamido group is directed toward esteratic site and forms hydrophobic contact with the indole ring of Trp 86 (3.82 Å).

Aroyl moieties of the both enantiomers of **5** form hydrophobic contacts with aromatic sidechains of Phe 297 (3.97 Å for (*R*) and 3.16 for (*S*)), Phe 338 (3.63 Å and 3.84 Å), and Tyr 341 (3.78 Å and 3.51 Å), Figure 9c and d. Aroyl carbonyl group of **5** (*R*) forms hydrogen bond with Tyr 124 –OH group (2.04 Å), and piperidine ring is accommodated below PAS residues (Tyr 124, Tyr 72, and Asp 74) and forms hydrophobic contact with Leu 76 side chain

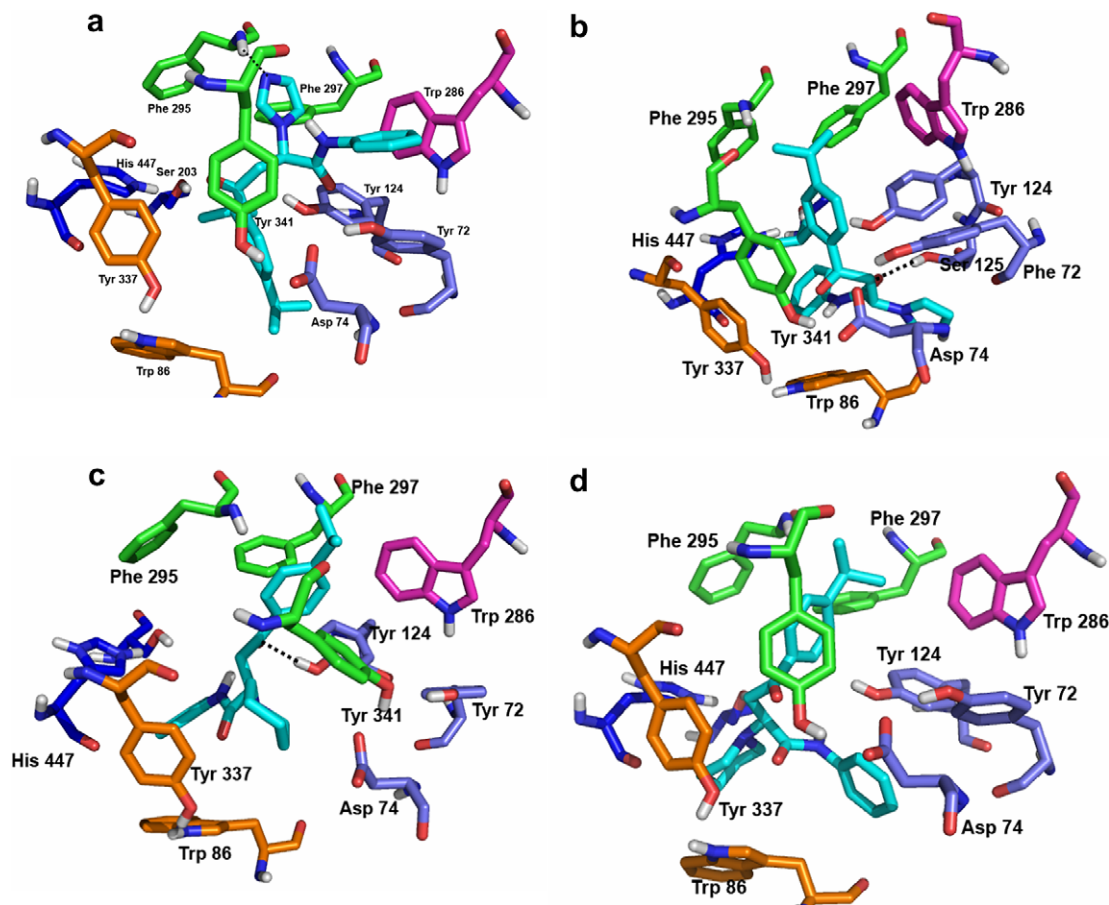


Figure 9. Compounds **5**(*R*), (a); **5**(*S*), (b); **19**(*R*), (c); and **19**(*S*), (d), docked into the binding site of the AChE, highlighting the protein residues that form the main interactions with the different structural units of the inhibitors. Hydrogen bonds are represented as black dots. Residues are colored as follows: anionic site Trp 86 and Tyr 337, orange; PAS Tyr 72, Asp 74, Tyr 124, Ser 125 violet and Trp 286 magenta; acyl binding pocket Tyr 341, Phe 297 and Phe 338 green; catalytic triad residues His 447 and Ser 203 dark blue; ligand, turquoise.

(4.70 Å). Phenylamido moiety of **5** (*R*) is directed toward catalytic triad residues (His 447 and Ser 203). Piperidine ring of **5** (*S*) is found near esteratic site and forms hydrophobic contact with Trp 86 (4.34 Å), while phenylamido group is directed toward Asp 74 and Ser 125.

Since **5** is the only compound that shows low micromolar activity toward both enzymes, we performed docking studies of **5** on HuBChE (PDB entry: 1POI) for making a comparison with their binding mode in AChE. Since there are less structural and molecular dynamics data for BChE we were not able to precisely decide which residues to keep flexible during calculation, and we performed classical rigid docking study. The best docked conformations obtained show that both enantiomers of **5** bind deeper inside BChE active site gorge than they do in AChE, Figure 10 a and b; the minimal distance between ligand and Ala 277 residue (homologous to Trp 286 of HuAChE) is 15 Å. This is probably a consequence of much wider BChE active site gorge, where six of the fourteen AChE aromatic amino acid residues (Tyr72, Tyr 124, Trp 286, Phe 295, Phe 297, and Tyr 337) are replaced by aliphatic in BChE (Asn 86, Gln 119, Ala 277, Leu 286, Val 288, and Ala 328). This causes 200 Å³ larger gorge in BChE than in AChE.⁴² Phenylamido groups of both enantiomers are accommodated in hydrophobic pocket, formed of side chains of the acyl pocket residues, Leu 286 and Val 288, and the three aromatic amino acids Trp 231, Phe 329, and Phe 398. Minimal distances between phenyl ring of **5** and these residues are in range between 3.29 and 4.16 Å. Amido carbonyl group of **5** (*R*) forms hydrogen bond with the side chain –OH group of the catalytic Ser 198 (analogous to Ser 203 in

HuAChE), 2.30 Å, while –*i*-Pr group forms hydrophobic contacts with the Tyr 332 side chain (analogous to Tyr 341 in HuAChE), 3.66 Å. Piperidine ring of **5** (*R*) is directed toward Tyr 128 (4.14 Å), near esteratic site and interacts with Trp 82 (4.85 Å, analogous to Trp 86 in HuAChE). Aroyl carbonyl group of **5** (*S*) enantiomer forms hydrogen bond with side chain –OH group of Ser 198 (1.96 Å, while piperidine ring is directed toward Tyr 332 (3.52 Å) and aroyl group is found near Trp 82 (3.82 Å) and Tyr 128 (4.38 Å) side chains.

3. Conclusions

In conclusion, 4-aryl-4-oxo-*N*-phenyl-2-aminy-substituted butyramides, novel type of reversible, moderately potent cholinesterase inhibitors, were designed, easily synthesized, and tested toward AChE and BChE. Appropriate substitution on aroyl moiety turns inactive compounds to moderately potent ones toward AChE, that is, small structural changes produce the increase of activity for ~2 orders of magnitude. Notably, change of piperidino methylene group by oxygen in morpholino derivatives produces inactive compounds toward AChE, but some of morpholino derivatives (**9** and **13**) are potent toward BChE. Those derivatives are selective inhibitors of BChE. Compounds **19** and **13** are the most potent inhibitors of AChE and BChE, respectively, acting in low micromolar concentrations, and also exert a linear mixed-type inhibition toward both enzymes. Alignment-independent 3D-QSAR analysis on set of the prepared and in the literature reported compounds, having compa-

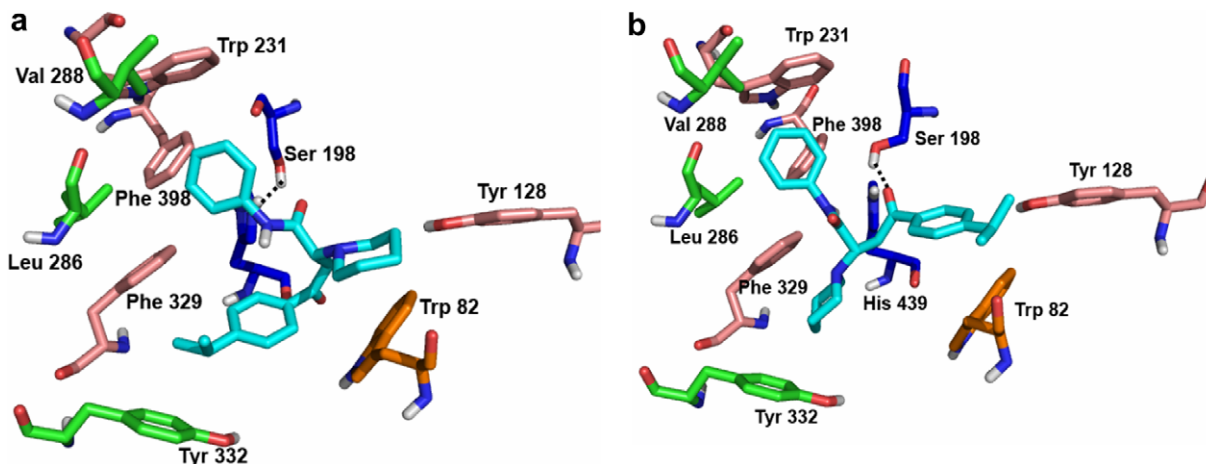


Figure 10. Compounds **5(R)**, (a); and **5(S)**, (b), docked into the binding site of BChE highlighting the protein residues that form the main interactions with the different structural units of the inhibitors. Hydrogen bonds are represented as dots.

rable potency toward *E. Eel* AChE, gives useful information for design novel, hopefully, more potent compounds. Existence of extended and properly directed hydrophobic moiety on aryl fragment is a requisite for potency. Docking studies showed that **5** and **19** bind, probably, in the middle of the gorge. Both enantiomers of **5** bind deeper inside BChE active site gorge, with binding conformations very distant from Ala 277; probably as a consequence of larger BChE gorge. Although moderately active, reported compounds will be used as templates for further structural modifications, based on the reported QSAR data. Further variation of aryl substitution, amidic portion of molecule and polymethylene chain of dimeric analogues (**21–26**) is planned, in order to find structural requirements needed for higher potency and better solubility.

4. Experimental

4.1. Chemistry

Melting points were measured in open capillary tubes on a SMP-10 Stuart apparatus and are uncorrected. Direct ESI-MS spectra were recorded on Agilent Technologies 6210-1210 TOF-LC-ESI-MS instrument in positive mode. ^1H and ^{13}C NMR spectra were recorded in CDCl_3 on Varian Gemini 200/50 MHz or Bruker AVANCE 500/125 MHz instruments. Chemical shifts are reported in parts per million (ppm) relative to tetramethylsilane (TMS) as the internal standard, and spin multiplicities are given as follows: s (singlet), d (doublet), t (triplet), m (multiplet), or br (broad).

4.1.1. General method to the synthesis of **1–26**

Briefly, 0.5–1.0 g of arylacrylic acid anilide (approximately 1.5–3.0 mmol) was dissolved or suspended in 10 mL of CHCl_3 , 20 mL of benzene was added and after 10 min of stirring, equimolar amount of the corresponding amine (piperidine, morpholine, or imidazole) was used to obtain compounds **1–20**. For compounds **21–26** half of equimolar amount of 1,8-diaminooctane was used in order to obtain dimeric compounds. For imidazole analogues **15–20**, 0.4 mL of triethylamine was added and the reaction mixture was refluxed for 3 h. The reaction mixture for all derivatives was stirred overnight at room temperature. After this the solvents were removed by spontaneous evaporation, or under the reduced pressure to low volume. The solid or semi-solid products were collected by vacuum suction and were characterized as described below. Interestingly, we found that further purification was not

necessary (except for **17** and **20**, which were recrystallized from acetone) and Michael addition gave almost quantitative yields for the majority of compounds. All obtained compounds were used in biological tests as the mixtures of enantiomers (**1–20**) or diastereomers (**21–26**). Reported ^1H NMR shifts of the A and B protons in ABX pattern correspond to dd centers, not real chemical shifts of the corresponding protons, for clarity.

4.1.1.1. Phenyl-4-oxo-*N*-phenyl-2-(*R,S*)-(1-piperidinyl)butyramide (**1**)

Starting from (*E*)-4-oxo-4-phenyl-2-butyric acid phenylamide (0.7 g, 2.78 mmol) and equimolar amount of piperidine, as described above, 0.56 g of **1** was obtained, 60.21% yield, pale yellow solid: mp 138–140 °C. ^1H NMR (200 MHz, CDCl_3) δ : 1.37 (br, 2H, piperidine $-\text{CH}_2-$); 1.52 (br, 4H, piperidine $-\text{CH}_2-$); 2.56 (br, 4H, piperidine $-\text{CH}_2-$); 3.09 (ABX, dd, $J_{1,2} = 3.65$ Hz, $J_{1,3} = 16.84$ Hz, 1H); 3.67, (ABX, dd, $J_{1,2} = 9.55$ Hz, $J_{1,3} = 16.85$ Hz, 1H); 4.01 (ABX, dd, $J_{1,2} = 3.37$ Hz, $J_{1,3} = 9.27$ Hz, 1H); 7.00, 7.04, 7.07 (triplet-like picks, 1H, amide *p*-phenyl); 7.25, 7.30, 7.33 (triplet-like picks, 2H, amide *m*-phenyl); 7.49–7.67 (overlapping multiplets, 5H, amide *o*-phenyl, aryl *p*-phenyl, aryl *m*-phenyl); 8.01, 8.04 (doublet-like picks, 2H, aryl *o*-phenyl); 10.62 (s, 1H, $-\text{NH}-$ amide). ^{13}C NMR (50 MHz, CDCl_3) δ : 24.17; 26.21; 34.64; 50.64; 65.34; 119.41; 123.36; 126.17; 128.17; 128.83; 133.25; 137.11; 139.06; 169.56; 198.96. LC ESI-MS (HR): MH^+ (obsd) 337.1916; calcd for $\text{C}_{21}\text{H}_{25}\text{N}_2\text{O}_2 = 337.1921$.

4.1.1.2. 4-(2,5-Dimethylphenyl)-4-oxo-*N*-phenyl-2-(*R,S*)-(1-piperidinyl)butyramide (**2**)

Starting from (*E*)-4-(2,5-dimethylphenyl)-4-oxo-2-butyric acid phenylamide (0.7 g, 2.50 mmol) and equimolar amount of piperidine, as described above, 0.75 g of **2** was obtained, 82.42% yield, yellow semi solid. ^1H NMR (200 MHz, CDCl_3) δ : 1.48 (m, 2H, piperidine $-\text{CH}_2-$); 1.65 (m, 4H, piperidine $-\text{CH}_2-$); 2.36 (s, 3H, *m*-CH₃); 2.48 (s, 3H, *o*-CH₃); 2.57 (t, 4H, $J_{1,2} = 5.07$ Hz, piperidine $-\text{CH}_2-$); 2.89 (ABX, dd, $J_{1,2} = 4.49$ Hz, $J_{1,3} = 16.85$ Hz, 1H); 3.55 (ABX, dd, $J_{1,2} = 8.43$ Hz, $J_{1,3} = 16.85$ Hz, 1H); 4.24 (ABX, dd, $J_{1,2} = 4.49$ Hz, $J_{1,3} = 7.86$ Hz, 1H); 7.04, 7.07, 7.11 (triplet-like picks, 1H, amide *p*-phenyl); 7.14–7.19 (m, 2H, amide *m*-phenyl); 7.24–7.35 (m, 2H, aryl *p*-phenyl, aryl *m*-phenyl); 7.53, 7.57 (m, 3H, amide *o*-phenyl, aryl *o*-phenyl); 9.42 (s, 1H, $-\text{NH}-$ amide). ^{13}C NMR (200 MHz, CDCl_3) δ : 20.56; 23.89; 26.66; 34.94; 51.05; 66.02; 119.19; 123.85; 128.27; 128.91; 131.64; 131.82; 134.77; 137.81; 138.30; 170.49; 202.36. LC ESI-MS (HR): MH^+ (obsd) 365.2239; calcd for $\text{C}_{23}\text{H}_{29}\text{N}_2\text{O}_2 = 365.2229$.

4.1.1.3. 4-(4-Chlorophenyl)-4-oxo-N-phenyl-2-(R,S)-(1-piperidinyl)butyramide (3). Starting from (*E*)-4-(4-chlorophenyl)-4-oxo-2-butenic acid phenylamide (1.0 g, 3.50 mmol) and equimolar amount of piperidine, as described above, 1.2 g of **3** was obtained, 92.30% yield, white solid: mp 134–136 °C. ¹H NMR (200 MHz, CDCl₃) δ: 1.48 (m, 2H, piperidine –CH₂–); 1.65 (m, 4H, piperidine –CH₂–); 2.57 (t, 4H, *J*_{1,2} = 4.91 Hz, piperidine –CH₂–); 2.84 (ABX, dd, *J*_{1,2} = 4.21 Hz, *J*_{1,3} = 16.29 Hz, 1H); 3.67 (ABX, dd, *J*_{1,2} = 7.86 Hz, *J*_{1,3} = 16.01 Hz, 1H); 4.26 (ABX, dd, *J*_{1,2} = 4.49 Hz, *J*_{1,3} = 8.14 Hz, 1H); 7.08 (t, 1H, *J*_{1,2} = 7.34 Hz, amide *p*-phenyl); 7.30 (t, 2H, *J*_{1,2} = 7.34 Hz, amide *m*-phenyl); 7.44 (d, 2H, *J* = 8.70 Hz, aryl *m*-phenyl); 7.52 (d, 2H, *J* = 7.61 Hz, amide *o*-phenyl); 7.97 (d, 2H, *J* = 8.70 Hz, aryl *o*-phenyl); 9.38 (s, 1H, –NH– amide). ¹³C NMR (200 MHz, CDCl₃) δ: 23.85; 26.62; 31.61; 51.09; 66.18; 119.22; 123.97; 128.18; 128.94; 129.71; 135.52; 137.65; 139.31; 170.33; 197.61. LC ESI-MS (HR): MH⁺ (obsd) 371.1530; calcd for C₂₁H₂₄ClN₂O₂ = 371.1526.

4.1.1.4. 4-(4-Methoxyphenyl)-4-oxo-N-phenyl-2-(R,S)-(1-piperidinyl)butyramide (4). Starting from (*E*)-4-(4-methoxyphenyl)-4-oxo-2-butenic acid phenylamide (1.0 g, 3.50 mmol) and equimolar amount of piperidine, as described above, 1.15 g of **4** was obtained, 89.84% yield, pale yellow solid: mp 112–114 °C. ¹H NMR (200 MHz, CDCl₃) δ: 1.47 (m, 2H, piperidine –CH₂–); 1.64 (m, 4H, piperidine –CH₂–); 2.58 (t, 4H, *J*_{1,2} = 5.03 Hz, piperidine –CH₂–); 2.94 (ABX, dd, *J*_{1,2} = 5.05 Hz, *J*_{1,3} = 16.85 Hz, 1H); 3.67 (ABX, dd, *J*_{1,2} = 7.30 Hz, *J*_{1,3} = 16.29 Hz, 1H); 3.86 (s, 3H, –OCH₃); 4.26 (ABX, dd, *J*_{1,2} = 5.05 Hz, *J*_{1,3} = 7.30 Hz, 1H); 6.94 (d, 2H, *J* = 8.70 Hz, aryl *m*-phenyl); 7.07 (t, 1H, *J*_{1,2} = 7.27 Hz, amide *p*-phenyl); 7.30 (t, 2H, *J*_{1,2} = 7.30 Hz, amide *m*-phenyl); 7.54 (d, 2H, *J* = 7.35 Hz, amide *o*-phenyl); 8.02 (d, 2H, *J* = 8.98 Hz, aryl *o*-phenyl); 9.38 (s, 1H, –NH– amide). ¹³C NMR (200 MHz, CDCl₃) δ: 23.89; 26.67; 31.57; 51.00; 55.39; 65.80; 113.67; 119.19; 123.85; 128.91; 130.06; 130.51; 137.81; 163.43; 170.64; 197.19. LC ESI-MS (HR): MH⁺ (obsd) 367.2032; calcd for C₂₂H₂₆N₂O₃ = 367.2022.

4.1.1.5. 4-(4-Isopropylphenyl)-4-oxo-N-phenyl-2-(R,S)-(1-piperidinyl)butyramide (5). Starting from (*E*)-4-(4-isopropylphenyl)-4-oxo-2-butenic acid phenylamide (1.0 g, 3.40 mmol) and equimolar amount of piperidine, as described above, 1.12 g of **5** was obtained, 87.50% yield, pale yellow solid: mp 90–91 °C. ¹H NMR (200 MHz, CDCl₃) δ: 1.27 (d, 6H, *J* = 6.72 Hz, *i*-PrCH₃); 1.40–1.72 (overlapping m, 6H, piperidine –CH₂–); 2.57 (t, 4H, *J*_{1,2} = 5.06 Hz, piperidine –CH₂–); 2.90–3.03 (overlapping m, 2H, ABX and *i*-PrCH); 3.70 (ABX, dd, *J*_{1,2} = 7.02 Hz, *J*_{1,3} = 16.57 Hz, 1H); 4.27 (ABX, dd, *J*_{1,2} = 5.06 Hz, *J*_{1,3} = 7.02 Hz, 1H); 7.07 (t, 1H, *J*_{1,2} = 7.20 Hz, amide *p*-phenyl); 7.26–7.35 (overlapping m, 4H, amide *m*-phenyl, and aryl *m*-phenyl); 7.52, 7.56 (doublet-like picks, 2H, amide *o*-phenyl); 8.97 (d, 2H, *J* = 8.98 Hz, aryl *o*-phenyl); 9.46 (s, 1H, –NH– amide). ¹³C NMR (200 MHz, CDCl₃) δ: 23.58; 23.89; 26.69; 31.83; 34.14; 51.02; 65.84; 119.20; 123.85; 126.63; 128.49; 134.94; 137.81; 154.42; 170.57; 198.33. LC ESI-MS (HR): MH⁺ (obsd) 379.2398; calcd for C₂₄H₃₁N₂O₂ = 379.2386.

4.1.1.6. 4-(2,4-Diisopropylphenyl)-4-oxo-N-phenyl-2-(R,S)-(1-piperidinyl)butyramide (6). Starting from (*E*)-4-(2,4-diisopropylphenyl)-4-oxo-2-butenic acid phenylamide (0.5 g, 1.49 mmol) and equimolar amount of piperidine, as described above, 0.62 g of **6** was obtained, 98.89% yield, pale yellow solid: mp 95–96 °C. ¹H NMR (500 MHz, CDCl₃) δ: 1.27 (d, 12H, *J* = 6.72 Hz, *i*-PrCH₃); 1.48 (m, 2H, piperidine –CH₂–); 1.65 (m, 4H, piperidine –CH₂–); 2.56 (t, 4H, *J*_{1,2} = 5.07 Hz, piperidine –CH₂–); 2.89–2.99 (overlapping m, 2H, ABX and *i*-PrCH); 3.41–3.60 (overlapping m, 2H, ABX and *i*-PrCH); 4.23 (ABX, dd, *J*_{1,2} = 4.38 Hz, *J*_{1,3} = 8.03 Hz, 1H); 7.04, 7.08 7.12 (triplet-like picks, 1H, amide *p*-phenyl); 7.27–7.36 (overlapping m, 4H, amide *m*-phenyl, and aryl *m*-phenyl); 7.53, 7.57

(doublet-like picks, 2H, amide *o*-phenyl); 7.67 (d, 1H, *J* = 7.97 Hz, aryl *o*-phenyl); 9.41 (s, 1H, –NH– amide). ¹³C NMR (125 MHz, CDCl₃) δ: 23.75; 23.97; 24.22; 24.40; 26.74; 29.17; 34.25; 36.06; 66.14; 119.19; 123.84; 124.66; 128.09; 128.92; 136.50; 137.87; 148.27; 151.96; 170.50; 203.17. LC ESI-MS (HR): MH⁺ (obsd) 421.2902; calcd for C₂₇H₃₇N₂O₂ = 421.2855.

4.1.1.7. 4-(5,6,7,8-Tetrahydro-2-naphthalenyl)-4-oxo-N-phenyl-2-(R,S)-(1-piperidinyl)butyramide (7). Starting from (*E*)-4-(5,6,7,8-tetrahydro-2-naphthalenyl)-4-oxo-2-butenic acid phenylamide (1.0 g, 3.50 mmol) and equimolar amount of piperidine, as described above, 1.25 g of **7** was obtained, 91.91% yield, pale brown solid: mp 92–94 °C. ¹H NMR (200 MHz, CDCl₃) δ: 1.49 (m, 2H, piperidine –CH₂–); 1.63 (m, 4H, piperidine –CH₂–); 1.79 (m, 4H, tetralinoyl –CH₂–); 2.57 (t, 4H, *J*_{1,2} = 5.05 Hz, piperidine –CH₂–); 2.79 (m, 4H, tetralinoyl –CH₂–); 2.96 (ABX, dd, *J*_{1,2} = 5.06, *J*_{1,3} = 16.29 Hz, 1H); 3.68 (ABX, dd, *J*_{1,2} = 6.74, *J*_{1,3} = 16.29 Hz, 1H); 4.26 (ABX, dd, *J*_{1,2} = 5.06, *J*_{1,3} = 7.30 Hz, 1H); 7.02–7.17 (overlapping m, 2H, aryl *m*-phenyl, and amide *p*-phenyl); 7.29 (t, 2H, *J*_{1,2} = 7.50 Hz, amide *m*-phenyl); 7.52, 7.56 (doublet-like picks, 2H, *J* = 7.84, amide *o*-phenyl); 7.73 (br, 2H, aryl *o*-phenyl); 9.47 (s, 1H, –NH– amide). ¹³C NMR (50 MHz, CDCl₃) δ: 22.82; 23.84; 26.64; 29.48; 31.81; 50.96; 65.73; 119.11; 123.76; 125.23; 128.82; 129.22; 134.44; 137.27; 137.78; 143.00; 170.55; 198.46. LC ESI-MS (HR): MH⁺ (obsd) 391.2393; calcd for C₂₅H₃₁N₂O₂ = 391.2386.

4.1.1.8. 4-Phenyl-4-oxo-N-phenyl-2-(R,S)-(4-morpholinyl)butyramide (8). Starting from (*E*)-4-oxo-4-phenyl-2-butenic acid phenylamide (0.5 g, 2.0 mmol) and equimolar amount of morpholine, as described above, 0.60 g of **8** was obtained, 88.63% yield, pale yellow solid: mp 144–146 °C. ¹H NMR (200 MHz, CDCl₃) δ: 2.66 (t, 4H, *J*_{1,2} = 4.45 Hz, morpholine –CH₂–); 3.00 (ABX, dd, *J*_{1,2} = 4.49 Hz, *J*_{1,3} = 16.28, 1H); 3.70–3.87 (overlapping m, 5H, morpholine –CH₂– and ABX); 4.30 (ABX, dd, *J*_{1,2} = 4.50 Hz, *J*_{1,3} = 7.30 Hz, 1H); 7.09 (triplet-like picks, 1H, *J*_{1,2} = 7.49 Hz amide *p*-phenyl); 7.31 (triplet-like picks, 2H, *J*_{1,2} = 7.69 Hz, amide *m*-phenyl); 7.43–7.62 (overlapping m, 5H, amide *o*-phenyl, aryl *m*-phenyl and aryl *p*-phenyl); 8.01–8.05 (m, 1H, aryl *o*-phenyl); 9.21 (s, 1H, –NH– amide). ¹³C NMR (50 MHz, CDCl₃) δ: 32.06; 50.00; 65.26; 67.31; 119.30; 124.19; 128.23; 128.69; 129.00; 133.19; 136.88; 137.52; 169.60; 198.17. LC ESI-MS (HR): MH⁺ (obsd) 339.1712; calcd for C₂₀H₂₃N₂O₃ = 339.1709.

4.1.1.9. 4-(2,5-Dimethylphenyl)-4-oxo-N-phenyl-2-(R,S)-(4-morpholinyl)butyramide (9). Starting from (*E*)-4-(2,5-dimethylphenyl)-4-oxo-2-butenic acid phenylamide (0.5 g, 1.80 mmol) and equimolar amount of morpholine, as described above, 0.64 g of **9** was obtained, 89.65% yield, yellow solid: mp 106–108 °C. ¹H NMR (200 MHz, CDCl₃) δ: 2.37 (s, 3H, *m*-CH₃); 2.47 (s, 3H, *o*-CH₃); 2.66 (t, 4H, *J*_{1,2} = 4.63 Hz, morpholine –CH₂–); 2.94 (ABX, dd, *J*_{1,2} = 4.49 Hz, *J*_{1,3} = 16.85 Hz, 1H); 3.60 (ABX, dd, *J*_{1,2} = 7.86, *J*_{1,3} = 16.28 Hz, 1H); 3.79 (*q*-like picks, 4H, *J*_{1,2} = 3.86, Hz, *J*_{1,3} = 7.91 Hz, morpholine –CH₂–); 4.26 (ABX, dd, *J*_{1,2} = 5.06 Hz, *J*_{1,3} = 7.86 Hz, 1H); 7.06–7.22 (overlapping m, 3H, amide *p*-phenyl, aryl *m*-phenyl and aryl *p*-phenyl); 7.26–7.36 (overlapping m, 2H, amide *m*-phenyl); 7.52–7.58 (overlapping m, 3H, amide *o*-phenyl and aryl *o*-phenyl); 9.20 (s, 1H, –NH–amide). ¹³C NMR (50 MHz, CDCl₃) δ: 20.63; 35.09; 50.04; 65.40; 67.33; 119.30; 124.17; 129.02; 131.77; 132.09; 134.94; 137.56; 137.96; 169.64; 201.77. LC ESI-MS (HR): MH⁺ (obsd) 367.2035; calcd for C₂₂H₂₇N₂O₃ = 367.2022.

4.1.1.10. 4-(4-Chlorophenyl)-4-oxo-N-phenyl-2-(R,S)-(4-morpholinyl)butyramide (10). Starting from (*E*)-4-(4-chlorophenyl)-4-oxo-2-butenic acid phenylamide (0.5 g, 1.70 mmol) and equi-

molar amount of morpholine, as described above, 0.56 g of **10** was obtained, 88.88% yield, white solid: mp 144–148 °C. ¹H NMR (200 MHz, CDCl₃) δ: 2.66 (t, 4H, *J*_{1,2} = 4.61 Hz, morpholine –CH₂–); 2.90 (ABX, dd, *J*_{1,2} = 4.49 Hz, *J*_{1,3} = 16.84 Hz, 1H); 3.71 (ABX, dd, partially overlapped with morpholine –CH₂–, *J*_{1,2} = 7.86 Hz, *J*_{1,3} = 16.28 Hz); 3.79 (*q*-like picks, 4H, *J*_{1,2} = 4.10 Hz, *J*_{1,3} = 8.45 Hz, morpholine –CH₂–); 4.29 (ABX, dd, *J*_{1,2} = 3.93 Hz, *J*_{1,3} = 7.87 Hz, 1H); 7.09 (t, 1H, *J*_{1,2} = 7.94 Hz, amide *p*-phenyl); 7.31 (t, 2H, *J*_{1,2} = 7.94 Hz, amide *m*-phenyl); 7.45 (d, 2H, *J* = 8.45 Hz, aryl *m*-phenyl); 7.50, 7.54 (doublet-like picks, 2H, *J* = 7.89 Hz, amide *o*-phenyl); 7.98 (d, 2H, *J* = 8.27 Hz, aryl *o*-phenyl); 9.17 (s, 1H, –NH– amide). ¹³C NMR (50 MHz, CDCl₃) δ 31.79; 49.96; 65.51; 67.28; 119.31; 124.28; 128.91; 129.09; 129.62; 135.28; 137.41; 139.58; 169.46; 197.04. LC ESI-MS (HR): MH⁺ (obsd) 373.1315; calcd for C₂₀H₂₂ClN₂O₃ = 373.1319.

4.1.1.11. 4-(4-Methoxyphenyl)-4-oxo-*N*-phenyl-2-(*R,S*)-(4-morpholinyl)butyramide (11). Starting from (*E*)-4-(4-methoxyphenyl)-4-oxo-2-butenic acid phenylamide (0.4 g, 1.42 mmol) and equimolar amount of morpholine, as described above, 0.52 g of **11** was obtained, 99.42% yield, pale yellow solid: mp 132–134 °C. ¹H NMR (200 MHz, CDCl₃) δ: 2.66 (t, 4H, *J*_{1,2} = 4.62 Hz, morpholine –CH₂–); 2.99 (ABX, dd, *J*_{1,2} = 4.81 Hz, *J*_{1,3} = 16.65 Hz, 1H); 3.65–3.85 (overlapped m, ABX and morpholine –CH₂–); 4.28 (ABX, dd, *J*_{1,2} = 4.98 Hz, *J*_{1,3} = 7.04 Hz, 1H); 6.95 (d, 2H, *J* = 8.89 Hz, aryl *m*-phenyl); 7.09 (t, 1H, *J*_{1,2} = 7.30 Hz, amide *p*-phenyl); 7.31 (t, 2H, *J*_{1,2} = 7.53 Hz, amide *m*-phenyl); 7.54 (d, 2H, *J* = 7.50 Hz, amide *o*-phenyl); 8.02 (d, 2H, *J* = 8.90 Hz, aryl *o*-phenyl); 9.23 (s, 1H, –NH–amide). ¹³C NMR (50 MHz, CDCl₃) δ 31.81; 50.02; 65.18; 67.35; 113.79; 119.28; 124.14; 128.98; 129.84; 130.53; 137.58; 163.59; 169.78; 196.57. LC ESI-MS (HR): MH⁺ (obsd) 381.2187; calcd for C₂₁H₂₅N₂O₄ = 381.2178.

4.1.1.12. 4-(4-Isopropylphenyl)-4-oxo-*N*-phenyl-2-(*R,S*)-(4-morpholinyl)butyramide (12). Starting from (*E*)-4-(4-isopropylphenyl)-4-oxo-2-butenic acid phenylamide (0.5 g, 1.70 mmol) and equimolar amount of morpholine, as described above, 0.61 g of **12** was obtained, 93.85% yield, pale yellow solid: mp 135–137 °C. ¹H NMR (200 MHz, CDCl₃) δ: 1.91 (d, 6H, *J* = 7.27 Hz, *i*-PrCH₃); 2.66 (t, 4H, *J*_{1,2} = 4.49 Hz, morpholine –CH₂–); 2.90–3.06 (overlapping m, 2H, *i*-PrCH and ABX); 3.68–3.85 (overlapping m, 5H, morpholine –CH₂– and ABX); 4.30 (ABX, dd, *J*_{1,2} = 5.05 Hz, *J*_{1,3} = 7.30 Hz, 1H); 7.09 (t, 1H, *J*_{1,2} = 7.21 Hz, amide *p*-phenyl); 7.26–7.35 (overlapping m, 4H, amide *m*-phenyl, and aryl *m*-phenyl); 7.54 (d, 2H, *J* = 7.94 Hz, amide *o*-phenyl); 7.98 (d, 2H, *J* = 8.48 Hz, aryl *o*-phenyl); 9.23 (s, 1H, –NH–amide). ¹³C NMR (50 MHz, CDCl₃) δ: 23.62; 32.05; 34.19; 50.04; 65.24; 67.37; 119.30; 124.17; 126.74; 128.51; 129.00; 134.70; 137.58; 154.75; 169.73; 197.79. LC ESI-MS (HR): MH⁺ (obsd) 369.1815; calcd for C₂₃H₂₉N₂O₃ = 369.1814.

4.1.1.13. 4-(2,4-Diisopropylphenyl)-4-oxo-*N*-phenyl-2-(*R,S*)-(4-morpholinyl)butyramide (13). Starting from (*E*)-4-(2,4-diisopropylphenyl)-4-oxo-2-butenic acid phenylamide (0.5 g, 1.50 mmol) and equimolar amount of morpholine, as described above, 0.51 g of **13** was obtained, 81.59% yield, white solid: mp 137–140 °C. ¹H NMR (200 MHz, CDCl₃) δ: 1.27 (d, 12H, *J* = 6.72 Hz, *i*-PrCH₃); 2.65 (t, 4H, *J*_{1,2} = 4.28 Hz, morpholine –CH₂–); 2.86–3.00 (overlapping m, 2H, *i*-PrCH and ABX); 3.40–3.64 (overlapping m, 2H, *i*-PrCH and ABX); 3.78 (*q*, 4H, *J*_{1,2} = 3.94 Hz, *J*_{1,3} = 7.87 Hz, morpholine –CH₂–); 4.26 (ABX, dd, *J*_{1,2} = 4.49 Hz, *J*_{1,3} = 8.42 Hz, 1H); 7.06–7.14 (overlapped m, 2H, amide *p*-phenyl and aryl *m*-phenyl); 7.26–7.36 (overlapped m, 3H, amide *m*-phenyl and aryl *m*-phenyl); 7.54 (d, 2H, *J* = 8.39 Hz, amide *o*-phenyl); 7.67 (d, 1H, *J* = 7.88 Hz, aryl *o*-phenyl); 9.18 (s, 1H, –NH– amide). ¹³C NMR (50 MHz, CDCl₃) δ: 23.73; 24.22; 24.31; 29.17; 34.25; 36.09; 50.03; 65.53;

67.35; 119.28; 123.28; 124.16; 124.76; 128.13; 129.02; 136.17; 137.61; 148.41; 152.27; 169.64; 202.65. LC ESI-MS (HR): MH⁺ (obsd) 423.2648; calcd for C₂₆H₃₅N₂O₃ = 423.2639.

4.1.1.14. 4-(5,6,7,8-Tetrahydro-2-naphthalenyl)-4-oxo-*N*-phenyl-2-(*R,S*)-(4-morpholinyl)butyramide (14). Starting from (*E*)-4-(5,6,7,8-tetrahydro-2-naphthalenyl)-4-oxo-2-butenic acid phenylamide (0.72 g, 2.40 mmol) and equimolar amount of morpholine, as described above, 0.84 g of **14** was obtained, 89.17% yield, pale yellow solid: mp 113–114 °C. ¹H NMR (200 MHz, CDCl₃) δ: 1.80 (m, 4H, tetralinoyl –CH₂–); 2.65 (t, 4H, *J*_{1,2} = 4.28 Hz, morpholine –CH₂–); 2.80 (br, 4H, tetralinoyl –CH₂–); 3.00 (ABX, dd, *J*_{1,2} = 4.99 Hz, *J*_{1,3} = 16.82 Hz, 1H); 3.65–3.79 (overlapped m, 5H, morpholine –CH₂– and ABX); 4.27 (ABX, dd, *J*_{1,2} = 5.19 Hz, *J*_{1,3} = 7.06 Hz, 1H); 7.04–7.35 (overlapped m, 4H, amide *p*-phenyl, amide *m*-phenyl and aryl *m*-phenyl); 7.51–7.56 (m, 2H, amide *o*-phenyl); 7.72–7.76 (m, 2H, aryl *o*-phenyl); 9.23 (s, 1H, –NH–amide). ¹³C NMR (50 MHz, CDCl₃) δ: 22.69; 22.82; 23.84; 23.64; 29.24; 29.48; 31.81; 50.96; 65.73; 119.11; 123.76; 123.23; 128.82; 129.05; 129.22; 134.44; 137.27; 137.78; 143.00; 170.55; 198.46. LC ESI-MS (HR): MH⁺ (obsd) 393.2163; calcd for C₂₄H₂₉N₂O₃ = 393.2178.

4.1.1.15. 4-(2,5-Dimethylphenyl)-4-oxo-*N*-phenyl-2-(*R,S*)-(1-imidazolyl)butyramide (15). Starting from (*E*)-4-(2,5-dimethylphenyl)-4-oxo-2-butenic acid phenylamide (0.5 g, 1.80 mmol) and equimolar amount of imidazole, as described above, 0.59 g of **15** was obtained, 95.16% yield, pale yellow solid: mp 156–160 °C. ¹H NMR (200 MHz, CDCl₃) δ: 2.34 (s, 3H, –CH₃); 2.37 (s, 3H, –CH₃); 3.46 (ABX, dd, *J*_{1,2} = 6.17 Hz, *J*_{1,3} = 17.97 Hz, 1H); 4.08 (ABX, dd, *J*_{1,2} = 7.87 Hz, *J*_{1,3} = 17.98 Hz, 1H); 5.63 (ABX, triplet, not resolved dd, *J*_{1,2} = 7.30 Hz, 1H); 7.05–7.36 (overlapping m, 7H, amide *p*-phenyl, amide *m*-phenyl, aryl *m*-phenyl, aryl *p*-phenyl, and imidazolyl CH); 7.49–7.59 (overlapped m, 4H, amide *o*-phenyl, aryl *o*-phenyl, and imidazolyl CH); 9.92 (s, 1H, –NH– amide). ¹³C NMR (50 MHz, CDCl₃) δ 20.83; 20.98; 44.26; 56.99; 117.95; 120.11; 124.67; 128.93; 129.51; 129.85; 132.11; 132.99; 135.48; 135.75; 136.01; 137.47; 137.83; 166.45; 199.53. LC ESI-MS (HR): MH⁺ (obsd) 348.1708; calcd for C₂₁H₂₂N₃O₂ = 348.1712.

4.1.1.16. 4-(4-Chlorophenyl)-4-oxo-*N*-phenyl-2-(*R,S*)-(1-imidazolyl)butyramide (16). Starting from (*E*)-4-(4-chlorophenyl)-4-oxo-2-butenic acid phenylamide (0.5 g, 1.70 mmol) and equimolar amount of imidazole, as described above, 0.55 g of **16** was obtained, 91.66% yield, pale yellow solid: mp 162–164 °C. ¹H NMR (500 MHz, CDCl₃) δ: 3.49 (ABX, dd, *J*_{1,2} = 5.67 Hz, *J*_{1,2} = 17.68 Hz, 1H); 4.11 (ABX, dd, *J*_{1,2} = 7.34 Hz, 18.01 Hz, 1H); 5.63 (ABX, triplet, not resolved dd, *J*_{1,2} = 6.00 Hz, 1H); 7.10–7.19 (overlapped m, 2H, amide *p*-phenyl and imidazolyl CH); 7.26–7.29 (overlapped m, 3H, amide-*m*-phenyl, and imidazolyl CH); 7.43 (d, 2H, *J* = 8.37 Hz, aryl *m*-phenyl); 7.50 (d, 2H, *J* = 7.39 Hz, amide *o*-phenyl); 7.67 (s, 1H, imidazolyl CH); 7.86 (d, 2H, *J* = 8.86 Hz, aryl *o*-phenyl); 9.09 (s, 1H, –NH– amide). ¹³C NMR (125 MHz, CDCl₃) δ: 41.84; 56.83; 117.91; 120.14; 124.96; 128.32; 129.00; 129.16; 129.54; 129.81; 133.88; 134.04; 137.34; 166.18; 194.84. LC ESI-MS (HR): MH⁺ (obsd) 354.1010; calcd for C₁₉H₁₇ClN₃O₂ = 354.1009.

4.1.1.17. 4-(4-Methoxyphenyl)-4-oxo-*N*-phenyl-2-(*R,S*)-(1-imidazolyl)butyramide (17). Starting from (*E*)-4-(4-methoxyphenyl)-4-oxo-2-butenic acid phenylamide (0.4 g, 1.42 mmol) and equimolar amount of imidazole, as described above, 0.19 g of **17** was obtained, 38.00% yield, white solid: mp 106–107 °C. ¹H NMR (200 MHz, CDCl₃) δ: 3.48 (ABX, dd, *J*_{1,2} = 5.62 Hz, *J*_{1,3} = 17.98 Hz, 1H); 3.84 (s, 3H, –OCH₃); 4.06 (ABX, dd, *J*_{1,2} = 7.86 Hz, *J*_{1,3} = 17.97 Hz, 1H); 5.72 (ABX, dd, *J*_{1,2} = 6.18 Hz, *J*_{1,3} = 7.87 Hz, 1H); 6.88 (d, 2H, *J* = 8.82 Hz, aryl *m*-phenyl); 7.05 (t, 1H, *J*_{1,2} = 7.18 Hz

amide *p*-phenyl); 7.14 (br, 1H, imidazolyl CH); 7.20–7.27 (overlapped *m*, 3H, amide-*m*-phenyl, and imidazolyl CH); 7.55 (d, 2H, $J = 7.41$ Hz amide *o*-phenyl); 7.68 (br, 1H, imidazolyl CH); 7.88 (d, 2H, $J = 8.91$ Hz aryl *o*-phenyl); 10.07 (s, 1H, –NH– amide). ^{13}C NMR (50 MHz, CDCl_3) δ 41.53; 55.48; 56.79; 113.91; 118.11; 120.08; 124.58; 128.87; 129.29; 130.49; 137.39; 137.87; 164.10; 166.60; 194.62. LC ESI-MS (HR): MH^+ (obsd) 350.1503; calcd for $\text{C}_{20}\text{H}_{20}\text{N}_3\text{O}_3 = 350.1505$.

4.1.1.18. 4-(4-Isopropylphenyl)-4-oxo-*N*-phenyl-2-(*R,S*)-(1-imidazolyl)butyramide (18). Starting from (*E*)-4-(4-isopropylphenyl)-4-oxo-2-butenic acid phenylamide (0.5 g, 1.70 mmol) and equimolar amount of imidazole, as described above, 0.55 g of **18** was obtained, 90.00% yield, pale yellow solid: mp 178 °C (decomp.). ^1H NMR (500 MHz, CDCl_3) δ 1.25 (d, 6H, $J = 7.07$ Hz, *i*-PrCH₃); 1.29 (d, 1H, $J = 7.07$ Hz, *i*-PrCH₃, other conformation); 2.96 (m, 1H, *i*-PrCH); 3.61 (ABX, dd, $J_{1,2} = 6.54$ Hz, $J_{1,3} = 18.17$ Hz, 1H); 4.09 (ABX, dd, $J_{1,2} = 6.90$ Hz, $J_{1,3} = 17.80$ Hz, 1H); 5.76 (ABX, triplet, not resolved dd, $J_{1,2} = 6.54$ Hz, 1H); 7.11–7.15 (overlapped *m*, 3H, amide *p*-phenyl, imidazolyl CH); 7.23 (s, 1H, imidazolyl CH); 7.29–7.31 (overlapped *m*, 4H, amide *m*-phenyl, and aryl *m*-phenyl); 7.53 (d, 2H, $J = 7.74$ Hz, amide *o*-phenyl); 7.86 (d, 2H, $J = 8.42$ Hz, aryl *o*-phenyl); 8.77 (s, 1H, –NH– amide). ^{13}C NMR (125 MHz, CDCl_3) δ : 22.57; 34.31; 47.72; 56.99; 114.54; 118.16; 120.14; 124.94; 126.93; 128.45; 129.00; 137.24; 137.49; 155.78; 166.37; 195.56. LC ESI-MS (HR): MH^+ (obsd) 362.1878; calcd for $\text{C}_{22}\text{H}_{24}\text{N}_3\text{O}_2 = 362.1869$.

4.1.1.19. 4-(2,4-Diisopropylphenyl)-4-oxo-*N*-phenyl-2-(*R,S*)-(1-imidazolyl) butyramide (19). Starting from (*E*)-4-(2,4-diisopropylphenyl)-4-oxo-2-butenic acid phenylamide (0.5 g, 1.50 mmol) and equimolar amount of imidazole, as described above, 0.58 g of **19** was obtained, 96.66% yield, white solid: 170 °C (decomp.). ^1H NMR (500 MHz, CDCl_3) δ : 1.14 (d, 3H, $J = 6.71$ Hz, *i*-PrCH₃); 1.19 (d, 3H, $J = 6.71$ Hz, *i*-PrCH₃); 1.25 (d, 6H, $J = 6.71$ Hz, *i*-PrCH₃); 2.99 (*h*, $J_{1,2} = 7.04$ Hz, $J_{1,3} = 14.09$ Hz, 1H, *i*-PrCH); 3.37 (*h*, 1H, $J_{1,2} = 7.04$ Hz, $J_{1,3} = 13.76$ Hz, *i*-PrCH); 3.45 (ABX, dd, $J_{1,2} = 6.38$ Hz, $J_{1,3} = 17.79$ Hz, 1H); 4.04 (ABX, dd, $J_{1,2} = 7.05$ Hz, $J_{1,3} = 17.79$ Hz, 1H); 5.59 (ABX, triplet, not resolved dd, $J_{1,2} = 6.71$ Hz, 1H); 7.09–7.13 (overlapped *m*, 2H, amide *p*-phenyl, and aryl *m*-phenyl); 7.15, 7.16 (doublet-like picks, 2H, imidazolyl CH); 7.25 (br, 1H imidazolyl CH); 7.29 (t, 2H, $J = 7.72$ Hz, amide *m*-phenyl); 7.48–7.55 (overlapped signals, 4H, aryl *m*-phenyl, amide *o*-phenyl, and aryl *o*-phenyl); 8.95 (s, 1H, –NH– amide). ^{13}C NMR (125 MHz, CDCl_3) δ : 23.68; 24.06; 29.11; 34.33; 45.29; 57.21; 117.84; 120.16; 123.47; 124.88; 124.98; 128.31; 128.98; 130.09; 134.43; 137.42; 137.55; 149.02; 153.29; 166.36; 200.57. LC ESI-MS (HR): MH^+ (obsd) 404.2340; calcd for $\text{C}_{25}\text{H}_{30}\text{N}_3\text{O}_2 = 404.2338$.

4.1.1.20. 4-(5,6,7,8-Tetrahydro-2-naphthalenyl)-4-oxo-*N*-phenyl-2-(*R,S*)-(1-imidazolyl)butyramide (20). Starting from (*E*)-4-(5,6,7,8-tetrahydro-2-naphthalenyl)-4-oxo-2-butenic acid phenylamide (0.5 g, 1.80 mmol) and equimolar amount of imidazole, as described above, 0.17 g of **20** was obtained, 25.37% yield, white solid: mp 154–156 °C. ^1H NMR (200 MHz, CDCl_3) δ 1.78 (br, 4H, tetralinoyl –CH₂–); 2.77 (br, 4H, tetralinoyl –CH₂–); 3.48 (ABX, dd, $J_{1,2} = 5.62$ Hz, $J_{1,3} = 17.97$ Hz, 1H); 4.09 (ABX, dd, $J_{1,2} = 7.86$ Hz, $J_{1,3} = 17.97$ Hz, 1H); 5.66 (ABX, triplet, not resolved dd, $J_{1,2} = 6.17$ Hz, 1H); 7.01–7.26 (overlapped *m*, 6H, amide *p*-phenyl, amide *m*-phenyl, aryl *m*-phenyl, and imidazolyl CH); 7.52–7.62 (overlapped *m*, 5H, amide *o*-phenyl, aryl *o*-phenyl, imidazolyl CH); 10.23 (s, 1H, –NH– amide). ^{13}C NMR (50 MHz, CDCl_3) δ : 22.61; 22.76; 29.22; 29.61; 41.77; 56.72; 118.08; 120.08; 124.54; 125.12; 128.85; 129.09; 133.24; 137.39; 137.92; 144.22; 166.62; 196.13. LC ESI-MS (HR): MH^+ (obsd) 374.1882; calcd for $\text{C}_{23}\text{H}_{24}\text{N}_3\text{O}_2 = 374.1869$.

4.1.1.21. 4-(2,5-Dimethylphenyl)-2-(*R,S*)-{7-[3-(*R,S*)-(2,5-dimethylphenyl)-3-oxo-1-phenylcarbamoyl-propylamino]-heptylamino}-4-oxo-*N*-phenyl-butylamide (21). Starting from (*E*)-4-(2,5-dimethylphenyl)-4-oxo-2-butenic acid phenylamide (0.4 g, 1.44 mmol) and a half of equimolar amount of 1,8-diaminooctane, as described above, 0.45 g of **21** was obtained, 88.23% yield, pale yellow semisolid. ^1H NMR (200 MHz, CDCl_3) δ : 1.33 (br, 8H, –CH₂–); 1.52 (br, 4H, –CH₂–); 2.60 (m, 2H, –CH₂–); 2.71 (m, 2H, –CH₂–); 2.34 (s, 6H, *m*-CH₃); 2.46 (s, 6H, *o*-CH₃); 3.25 (ABX, dd, $J_{1,2} = 8.42$ Hz, $J_{1,3} = 17.41$ Hz, 2H); 3.55 (ABX, dd, $J_{1,2} = 3.37$ Hz, $J_{1,3} = 17.41$ Hz, 2H); 3.68 (ABX, dd, $J_{1,2} = 3.37$ Hz, $J_{1,3} = 8.42$ Hz, 2H); 7.05–7.21 (overlapped *m*, 6H, amide *p*-phenyl, aryl *p*-phenyl); 7.26–7.36 (overlapped *m*, 6H, amide *m*-phenyl, aryl *m*-phenyl); 7.53–7.61 (overlapped *m*, 4H, amide *o*-phenyl, aryl *o*-phenyl); 9.59 (s, 1H, –NH– amide). ^{13}C NMR (50 MHz, CDCl_3) δ 20.83; 21.05; 27.17; 29.39; 30.22; 42.55; 48.36; 59.59; 119.24; 124.05; 128.31; 128.98; 129.62; 132.04; 132.64; 135.43; 136.66; 137.76; 171.92; 202.34. LC ESI-MS (HR): MH^+ (obsd) 703.4223; calcd for $\text{C}_{43}\text{H}_{53}\text{N}_4\text{O}_4 = 703.4221$, MH_2^{2+} (obsd) 352.2145; calcd for $\text{C}_{43}\text{H}_{54}\text{N}_4\text{O}_4 = 352.2136$.

4.1.1.22. 4-(4-Chlorophenyl)-2-(*R,S*)-{7-[3-(*R,S*)-(4-chlorophenyl)-3-oxo-1-phenylcarbamoyl-propylamino]-heptylamino}-4-oxo-*N*-phenyl-butylamide (22). Starting from (*E*)-4-(4-chlorophenyl)-4-oxo-2-butenic acid phenylamide (0.5 g, 1.70 mmol) and a half of equimolar amount of 1,8-diaminooctane, as described above, 0.56 g of **22** was obtained, 91.80% yield, white solid: mp 101 °C (decomp.). ^1H NMR (500 MHz, CDCl_3) δ : 1.31–1.36 (m, 8H, –CH₂–); 1.48–1.52 (m, 4H, –CH₂–); 2.55–2.60 (m, 2H, –CH₂–); 2.69–2.74 (m, 2H, –CH₂–); 3.30 (ABX, dd, $J_{1,2} = 8.44$ Hz, $J_{1,3} = 17.61$ Hz, 2H); 3.58 (ABX, dd, $J_{1,2} = 3.30$ Hz, $J_{1,3} = 17.61$ Hz, 2H); 3.68 (ABX, dd, $J_{1,2} = 3.30$ Hz, $J_{1,3} = 8.07$ Hz, 2H); 7.10 (t, 2H, $J = 7.21$ Hz, amide *p*-phenyl); 7.32 (t, 4H, $J = 7.76$ Hz, amide *m*-phenyl); 7.44 (d, 4H, $J = 8.87$ Hz, aryl *m*-phenyl); 7.57 (d, 4H, $J = 7.77$ Hz, amide *o*-phenyl); 7.91 (d, 4H, $J = 8.87$ Hz, aryl *o*-phenyl); 10.23 (s, 1H, –NH– amide). ^{13}C NMR (125 MHz, CDCl_3) δ 26.91; 29.11; 29.96; 39.61; 48.11; 59.09; 119.09; 123.90; 128.05; 128.80; 129.34; 134.37; 137.42; 139.86; 171.34; 197.17. LC ESI-MS (HR): MH^+ (obsd) 715.2821; calcd for $\text{C}_{39}\text{H}_{43}\text{Cl}_2\text{N}_4\text{O}_4 = 715.2821$; MH_2^{2+} (obsd) 388.1452; calcd for $\text{C}_{39}\text{H}_{43}\text{Cl}_2\text{N}_4\text{O}_4 = 358.1443$.

4.1.1.23. 4-(4-Methoxyphenyl)-2-(*R,S*)-{7-[3-(*R,S*)-(4-methoxyphenyl)-3-oxo-1-phenylcarbamoyl-propylamino]-heptylamino}-4-oxo-*N*-phenyl-butylamide (23). Starting from (*E*)-4-(4-methoxyphenyl)-4-oxo-2-butenic acid phenylamide (0.3 g, 1.10 mmol) and a half of equimolar amount of 1,8-diaminooctane, as described above, 0.38 g of **23** was obtained, 97.43% yield, pale yellow semisolid: mp 87–89 °C. ^1H NMR (500 MHz, CDCl_3) δ 1.30–1.35 (m, 8H, –CH₂–); 1.47–1.51 (m, 4H, –CH₂–); 2.54–2.59 (m, 2H, –CH₂–); 2.69–2.74 (m, 2H, –CH₂–); 3.24 (ABX, dd, $J_{1,2} = 7.44$ Hz, $J_{1,3} = 18.87$ Hz, 2H); 3.57 (ABX, dd, $J_{1,2} = 3.30$ Hz, $J_{1,3} = 17.24$ Hz, 2H); 3.66 (ABX, dd, $J_{1,2} = 2.93$ Hz, $J_{1,3} = 8.43$ Hz, 2H); 6.92 (d, 4H, $J = 8.87$ Hz, aryl *m*-phenyl); 7.09 (t, 2H, $J = 7.54$ Hz, amide *p*-phenyl); 7.32 (t, 4H, $J = 7.54$ Hz, amide *m*-phenyl); 7.59 (d, 4H, $J = 8.01$ Hz, amide *o*-phenyl); 7.95 (d, 4H, $J = 8.95$ Hz, aryl *o*-phenyl); 9.64 (s, 1H, –NH– amide). ^{13}C NMR (125 MHz, CDCl_3) δ : 27.17; 29.34; 30.20; 39.81; 48.44; 55.45; 59.58; 113.83; 119.23; 124.00; 128.27; 128.93; 130.48; 137.78; 163.84; 171.91; 196.97. LC ESI-MS (HR): MH^+ (obsd) 707.3804; calcd for $\text{C}_{41}\text{H}_{48}\text{N}_4\text{O}_4 = 707.3809$, MH_2^{2+} (obsd) 354.1956; calcd for $\text{C}_{39}\text{H}_{43}\text{Cl}_2\text{N}_4\text{O}_4 = 354.1938$.

4.1.1.24. 4-(4-Isopropylphenyl)-2-(*R,S*)-{7-[3-(*R,S*)-(4-isopropylphenyl)-3-oxo-1-phenylcarbamoyl-propylamino]-heptylamino}-4-oxo-*N*-phenyl-butylamide (24). Starting from (*E*)-4-(4-isopropylphenyl)-4-oxo-2-butenic acid phenylamide (0.5 g, 1.70 mmol)

and a half of equimolar amount of 1,8-diaminooctane, as described above, 0.58 g of **24** was obtained, 93.55% yield, pale yellow solid: mp 92–94 °C. ^1H NMR (200 MHz, CDCl_3) δ 1.26 (d, $J = 6.74$ Hz, 12H, *i*-PrCH₃); 1.31 (br, 8H, $-\text{CH}_2-$); 1.50 (br, 8H, $-\text{CH}_2-$); 2.50–2.75 (m, 4H, $-\text{CH}_2-$); 3.28 (ABX, dd, $J_{1,2} = 5.05$ Hz, $J_{1,3} = 16.56$ Hz, 2H); 3.70, (ABX, dd, $J_{1,2} = 7.02$ Hz, $J_{1,3} = 16.57$ Hz, 2H); 4.27 (ABX, dd, $J_{1,2} = 5.06$ Hz, $J_{1,3} = 7.02$ Hz, 2H); 7.05, 7.09, 7.12 (triplet-like picks, 2H, amide *p*-phenyl); 7.25–7.36 (overlapped m, 4H, amide *m*-phenyl and aryl *m*-phenyl); 7.57, 7.61 (doublet-like picks, 4H, amide *o*-phenyl); 7.92 (d, 4H, $J = 8.95$ Hz, aryl *o*-phenyl); 9.61 (s, 2H, $-\text{NH}-$ amide). ^{13}C NMR (50 MHz, CDCl_3) δ : 23.54; 27.13; 29.33; 30.17; 34.19; 39.97; 48.38; 59.41; 119.24; 126.80; 128.29; 128.44; 128.96; 134.13; 137.76; 155.22; 171.95; 198.206. LC ESI-MS (HR): MH^+ (obsd) 731.4536; calcd for $\text{C}_{45}\text{H}_{57}\text{N}_4\text{O}_4 = 731.4519$; MH_2^{2+} (obsd) 366.2302; calcd for $\text{C}_{45}\text{H}_{58}\text{N}_4\text{O}_4 = 366.2294$.

4.1.1.25. 4-(2,4-Diisopropylphenyl)-2-(*R,S*)-[7-[3-(*R,S*)-(4-isopropylphenyl)-3-oxo-1-phenylcarbamoyl-propylamino]-heptylamino]-4-oxo-*N*-phenyl-butylamide (25). Starting from (*E*)-4-(2,4-diisopropylphenyl)-4-oxo-2-butenoic acid phenylamide (0.5 g, 1.50 mmol) and a half of equimolar amount of 1,8-diaminooctane, as described above, 0.56 g of **25** was obtained, 91.80% yield, pale yellow semisolid: mp 69–70 °C. ^1H NMR (500 MHz, CDCl_3) δ : 1.23–1.26 (br, 24H, *i*-PrCH₃); 1.34 (br, 8H, $-\text{CH}_2-$); 1.53 (br, 8H, $-\text{CH}_2-$); 2.56–2.76 (m, 4H, $-\text{CH}_2-$); 3.24 (ABX, dd, $J_{1,2} = 8.07$ Hz, $J_{1,3} = 17.24$ Hz, 2H); 3.47–3.51 (ABX, *m*, 2H); 3.67 (ABX, dd, $J_{1,2} = 3.30$ Hz, $J_{1,3} = 7.70$ Hz, 2H); 7.07, 7.09, 7.10 (triplet-like picks, 2H, amide *p*-phenyl); 7.26 (br, 2H, aryl *m*-phenyl); 7.29–7.33 (overlapped signals, 8H, aryl *m*-phenyl, amide *o*-phenyl, and aryl *o*-phenyl); 9.54 (s, 1H, $-\text{NH}-$ amide). ^{13}C NMR (125 MHz, CDCl_3) δ : 23.68; 24.20; 27.23; 29.20; 29.43; 30.29; 34.27; 43.51 48.39; 59.75; 119.26; 13.38; 124.02; 124.87; 126.40; 128.95; 135.16; 137.78; 148.66; 152.79; 171.74; 203.48. LC ESI-MS (HR): MH^+ (obsd) 815.5471; calcd for $\text{C}_{51}\text{H}_{69}\text{N}_4\text{O}_4 = 815.5475$, MH_2^{2+} (obsd) 408.2781; calcd for $\text{C}_{51}\text{H}_{70}\text{N}_4\text{O}_4 = 408.2771$.

4.1.1.26. 4-(5,6,7,8-Tetrahydro-2-naphthalenyl)-2-(*R,S*)-[7-[3-(*R,S*)-(5,6,7,8-tetrahydro-2-naphthalenyl)-3-oxo-1-phenylcarbamoyl-propylamino]-heptylamino]-4-oxo-*N*-phenyl-butylamide (26). Starting from (*E*)-4-(2,4-diisopropylphenyl)-4-oxo-2-butenoic acid phenylamide (0.5 g, 1.80 mmol) and a half of equimolar amount of 1,8-diaminooctane, as described above, 0.57 g of **26** was obtained, 83.82% yield, pale yellow semisolid. ^1H NMR (200 MHz, CDCl_3) δ : 1.30 (br, 8H, $-\text{CH}_2-$); 1.49 (br, 4H, $-\text{CH}_2-$); 1.79 (br, 8H, tetralinoyl $-\text{CH}_2-$); 2.58, 2.68 (br, 4H, overlapped broad multiplets, $-\text{CH}_2-$); 2.79 (br, 8H, tetralinoyl $-\text{CH}_2-$); 3.25 (ABX, dd, $J_{1,2} = 8.43$ Hz, $J_{1,3} = 16.85$ Hz, 2H); 3.56–4.11 (ABX, *m*, 4H); 7.05–7.15 (4H, overlapping multiplets, amide *p*-phenyl, aryl *m*-phenyl); 7.25, 7.28, 7.32 (triplet-like picks, 4H, amide *m*-phenyl); 7.57–7.70 (overlapping multiplets, aryl *o*-phenyl, aryl *m*-phenyl); 9.61 (s, 1H, $-\text{NH}-$ amide). ^{13}C NMR (50 MHz, CDCl_3) δ : 22.65; 22.79; 27.11; 29.24; 29.33; 29.57; 30.17; 40.02; 48.38; 59.45; 119.20; 123.99; 125.18; 128.27; 128.94; 129.45; 133.75; 137.76; 143.82; 171.99; 198.44. LC ESI-MS (HR): MH^+ (obsd) 755.4536; calcd for $\text{C}_{47}\text{H}_{56}\text{N}_4\text{O}_4 = 755.4535$, MH_2^{2+} (obsd) 378.2302; calcd for $\text{C}_{47}\text{H}_{56}\text{N}_4\text{O}_4 = 378.2298$.

4.2. Biological studies

The inhibition potency of the prepared compounds on acetylcholinesterase (AChE) activity was evaluated spectrophotometrically by the method of Ellman et al.,³¹ using AChE from *E. Eel*, type VI-S (Sigma) and acetylcholine iodide (0.28 mM) as substrates. Four to six different concentrations, which produce 20–80% of enzyme activity inhibition, of the each compound were used. The

reaction took place in final volume of 2 mL of 0.1 M potassium phosphate buffer, pH 8.0, containing 0.03 units of AChE and 0.3 mM 5,5'-dithiobis(2-nitrobenzoic)acid (DTNB), used to produce yellow anion of 5-thio-2-nitrobenzoic acid in reaction with thiocholine released by AChE. Test compound was added to the enzyme solution and preincubated at 25 °C for 35 min followed by the addition of DTNB (0.95 mL) and substrate (50 μL). Inhibition curves were performed at least in triplicate. One triplicate sample without test compound was always present to yield the 100% of AChE activity. The reaction was monitored for 3 min, and the color production was measured at 412 nm. The reaction rates were compared, and the percent inhibition, due to the presence of test compounds, was calculated. IC_{50} values were determined from inhibition curves (log inhibitor concentration vs percent inhibition).

The investigation of butyrylcholinesterase (BChE) inhibition was carried out similarly, using 0.035 units of horse serum BChE (Fluka) and 0.5 mM butyrylthiocholine iodide instead of AChE and acetylthiocholine, in final volume of 2 mL. For determination of inhibition type of **19** toward AChE and **13** toward BChE, the Lineweaver–Burk plots were generated by using a fixed amount of cholinesterase and varying amounts of the substrate (0.10–0.20 mM, AChE and 0.11–0.33 mM, BChE) in the absence or presence of different inhibitor concentrations. The re-plot of the slopes of the double reciprocal plots against inhibitor concentration gave the inhibitor constant (K_i) as the intercept on the x-axis.

4.3. 3D-QSAR methods

SMILES notation of all compounds used in model were converted to 3D by OMEGA,⁴³ using MMFF94s⁴⁴ force field (build and search), and five lowest energy conformations per compound were generated. Every conformer was further minimized by semi-empirical MO PM6 method,⁴⁵ using implicit solvation (water) and the structure of each compound having the lowest heat of formation was used for model building. Protonation state of each compound was ascribed by Pentacle under pH value reported in the original reference (8.00). Pentacle use AMANDA⁴⁶ algorithm to produce second generation alignment-independent molecular descriptors (GRIND-2), insensitive to small to medium conformational changes, derived from GRID⁴⁷ molecular interaction fields (MIFs). Derived GRID MIF minima are encoded in variables that describe pair of nodes (IE of each node and the corresponding distance between nodes); descriptors are further processed by means of built-in PCA/PLS (principal component analysis/partial least squares) chemometric tool.

For model generation N1, O, and DRY probes were used, with GRID resolution of 0.4 Å. For encoding, maximum auto and cross-correlation were applied (MACC2). Probes cut-off was hold on default value, as well as MACC2 smoothing window and scale factor. Validation of model was done by cross-validation using three groups of approximately the same size in which the objects were assigned randomly. For the final model leave two out and leave one out cross-validation data are also reported. Due to unavailability of the current Pentacle prerelease to show interaction energies (IE) on a particular node, their values were estimated by GRID. DRY probe isovolumes were extracted by BIOCUBE.⁴⁸

To examine influence of the grid resolution, as well as influence of the alignment of compounds on the reported model, few more models were built using: (a) different grid resolutions (0.2, 0.7, and 1.0 Å) and (b) alignment of compounds within the each subset; with retaining of all other parameters as for the reported model. In this way the obtained patterns of PLS coefficient plots were slightly different, but variables that have high influence on the each model obtained were exactly the same as those described in the reported model. So, it has been confirmed that method used is very robust in respect to grid resolution and the alignment independent.

4.4. Docking procedures

All docking experiments were performed on the *Mus Musculus* AChE refined at 2.05 Å resolution (PDB entry: 2HA2). Truncated residues were properly completed by means of Swiss PDB Viewer.⁴⁹ Hydrogen atoms were added to the protein amino acid residues, non-polar hydrogens were merged, and Gasteiger charges were loaded using AUTODOCK Tools.⁵⁰ The lowest energy conformations of **5** (R) and **19** (R) were generated using Omega software⁴³ and further optimized by PM6 semiempirical MO method⁴⁵ as implemented in MOPAC2009. VEGA ZZ 2.3.1⁵¹ was used as GUI. Conformations of **5** (S) and **19** (S) were generated as mirror images of R configurations using VEGA ZZ. Both enantiomers of both compounds were docked to mAChE using AUTODOCK 4.0.1 package.³⁸ Docking was carried out by using the hybrid Lamarckian genetic algorithm, 50 runs were performed with an initial population of 250 randomly placed individuals and maximum number of 1.0×10^7 energy evaluations. Resulting docked orientations within RMSD of 0.5 Å were clustered together. All other parameters were maintained at their default settings. The lowest energy cluster returned by AUTODOCK for each compound was used for further analysis. Docking on HuBChE is performed under the same conditions, except that no amino acid residues were held flexible during calculation.

Acknowledgments

Ministry of Science and Technological Development of the Republic of Serbia supports this work (Grants: 142010 and 142020). B.J.D. gratefully acknowledges OpenEye Scientific Software for OMEGA license.

Supplementary data

Supplementary data associated with this article can be found, in the online version, at doi:10.1016/j.bmc.2009.12.042.

References and notes

- Terry, A. V., Jr.; Buccafusco, J. J. *J. Pharm. Exp. Ther.* **2003**, *306*, 821.
- Gibney, G.; Camp, S.; Dionne, M.; MacPhee-Quigley, K.; Taylor, P. *Proc. Natl. Acad. Sci. U.S.A.* **1990**, *87*, 7546.
- Shafferman, A.; Velan, B.; Ordentlich, A.; Kronman, C.; Grosfeld, H.; Leitner, M.; Flashner, Y.; Cohen, S.; Barak, D.; Naomi, A. *EMBO J.* **1992**, *11*, 3561.
- Radić, Z.; Gibney, G.; Kawamoto, S.; MacPhee-Quigley, K.; Bongiorno, C.; Taylor, P. *Biochemistry* **1992**, *31*, 9760.
- Ekholm, M.; Korschin, H. J. *Mol. Struct., Theochem.* **1990**, *467*, 161.
- Ordentlich, A.; Barak, D.; Kronman, C.; Ariel, N.; Segall, Y.; Velan, B.; Shafferman, A. *J. Biol. Chem.* **1998**, *273*, 19509.
- Kreienkamp, H. J.; Weise, C.; Raba, R.; Aaviksar, A.; Hucko, F. *Proc. Natl. Acad. Sci. U.S.A.* **1991**, *88*, 6117.
- Weise, C.; Kreienkamp, H. J.; Raba, R.; Pedak, A.; Aaviksar, A.; Hucko, F. *EMBO J.* **1990**, *9*, 3385.
- Sussman, J. L.; Harel, M.; Frolow, F.; Oefner, C.; Goldman, A.; Toker, L.; Silman, I. *Science* **1991**, *253*, 872.
- Ordentlich, A.; Barak, D.; Kronman, C.; Flashner, U.; Leitner, M.; Segall, Y.; Ariel, N.; Cohen, S.; Velan, B.; Shafferman, A. *J. Biol. Chem.* **1993**, *268*, 17083.
- Vellom, D. C.; Radić, Z.; Ying, L.; Pickering, N. A.; Camp, S.; Taylor, P. *Biochemistry* **1993**, *32*, 12.
- Taylor, P.; Lappi, S. *Biochemistry* **1975**, *14*, 1989.
- Barak, D.; Kronman, C.; Ordentlich, A.; Naomi, A.; Bromberg, A.; Marcus, D.; Lazar, A.; Velan, B.; Shafferman, A. *J. Biol. Chem.* **1994**, *269*, 6296.
- Bourne, Y.; Taylor, P.; Radić, Z.; Marchot, P. *EMBO J.* **2003**, *22*, 1.
- Bartolini, M.; Bertucci, C.; Cavrini, V.; Andrisano, V. *Biochem. Pharmacol.* **2003**, *65*, 407.
- Inestrosa, N. C.; Alvarez, A.; Perez, A. C.; Moreno, R. D.; Vicente, M.; Linker, C.; Casanueva, O. I.; Soto, C.; Garrido, J. *Neuron* **1996**, *16*, 881.
- Mesulam, M. M.; Guillozet, A.; Show, P.; Levey, A.; Duysen, E. G. M.; Lockridge, O. *Neuroscience* **2002**, *110*, 627.
- Li, B.; Stribley, J. A.; Ticu, A.; Xie, W.; Shopfer, L. M.; Hammond, P.; Brimjoin, S.; Hinrichs, S. H.; Lockridge, O. *J. Neurochem.* **2000**, *75*, 1320.
- Jhee, S. S.; Shiovitz, T.; Hartman, R. D.; Mesina, J.; Anand, R.; Sramek, J.; Cutler, N. R. *Neuropharmacology* **2002**, *25*, 122.
- Perry, E. K.; Perry, R. H.; Blessed, G.; Tomlinson, B. E. *Neuropathol. Appl. Neurobiol.* **1978**, *4*, 273.
- Hasan, A.; Khan, K. M.; Sher, M.; Maharvi, G. M.; Nawaz, S. A.; Choudhary, M. I.; Rahman, A. U.; Supuran, C. T. *J. Enzyme Inhib. Med. Chem.* **2005**, *20*, 41.
- Trujillo-Ferrara, J.; Montoya Cano, L.; Espinoza-Fonseca, M. *Bioorg. Med. Chem. Lett.* **2003**, *13*, 1825.
- Correa-Basurto, J.; Alcantara, I. V.; Espinoza-Fonseca, M.; Trujillo-Ferrara, J. G. *Eur. J. Med. Chem.* **2005**, *40*, 732.
- Correa-Basurto, J.; Espinoza-Raya, J.; Gonzalez-May, M.; Espinoza-Fonseca, L. M.; Vasquez-Alcantara, I.; Trujillo-Ferrara, J. *J. Enzyme Inhib. Med. Chem.* **2006**, *21*, 133.
- Correa-Basurto, J.; Flores-Sandoval, C.; Marin-Cruz, J.; Royo-Dominguez, A.; Espinoza-Fonseca, L. M.; Trujillo-Ferrara, J. G. *Eur. J. Med. Chem.* **2007**, *42*, 10.
- Viegas, C.; Bolzani, V. S.; Pimentel, L. S. B.; Castro, N. G.; Cabral, R. F.; Costa, R. S.; Floyd, C.; Rocha, M. S.; Young, M. C. M.; Barreiro, E. J.; Fraga, C. A. M. *Bioorg. Med. Chem.* **2005**, *13*, 4184.
- Kwon, Y. E.; Park, J. Y.; No, K. T.; Shin, J. H.; Lee, S. K.; Eun, J. S.; Yang, J. H.; Shin, T. Y.; Kim, D. K.; Chae, B. S.; Leem, J. Y.; Kim, K. H. *Bioorg. Med. Chem.* **2007**, *15*, 6596.
- Sadashiva, C. T.; Chandra, J. N. N. S.; Ponnappa, K. C.; Gowda, T. V.; Rangappa, K. S. *Bioorg. Med. Chem. Lett.* **2006**, *16*, 3932.
- Toda, N.; Tago, K.; Marumoto, S.; Takami, K.; Ori, M.; Yamada, N.; Koyama, K.; Naruto, S.; Abe, K.; Yamazaki, R.; Hara, T.; Aoyagi, A.; Abe, Y.; Kaneko, T.; Kogen, H. *Bioorg. Med. Chem.* **2003**, *11*, 1935.
- Rodriguez-Franco, M. I.; Fernandez-Bachiller, M. I.; Perez, C.; Castro, A.; Martinez, A. *Bioorg. Med. Chem.* **2005**, *13*, 6795.
- Ellman, L. G.; Courtney, K. D.; Andres, V., Jr.; Featherstone, M. R. *Biochem. Pharmacol.* **1961**, *2*, 88.
- Papa, D.; Schwenk, E.; Villani, F.; Klingsberg, E. *J. Am. Chem. Soc.* **1948**, *70*, 3356.
- Kulsa, P.; Hoff, D. R.; Mrozik, H. H., U.S. Pat. 4,130,661, Merck & Co., Inc. Rahway, N.J., 1977.
- Lee, S.-S.; Venkatesham, U.; Prasad Rao, C. P.; Lam, S.-H.; Lin, J.-H. *Bioorg. Med. Chem.* **2007**, *15*, 1034.
- Chiou, C.-M.; Kang, J.-J.; Lee, S.-S. *J. Nat. Prod.* **1998**, *61*, 46.
- Rangappa, K. S. B. *J. Phys. Org. Chem.* **2005**, *18*, 773.
- Benaka Prasad, S. B.; Sunil Kumar, Y. C.; Ananda Kumar, C. S.; Sadashiva, C. T.; Vinaya, K.; Rangappa, K. S. *Open Med. Chem. J.* **2007**, *1*, 4.
- Morris, G. M.; Goodsell, D. S.; Halliday, R. S.; Huey, R.; Hart, W. E.; Belew, R. K.; Olson, A. J. *J. Comput. Chem.* **1998**, *19*, 1639.
- Cavalli, A.; Bottegoni, B.; Raco, C.; De Vivo, M.; Recanatini, M. *J. Med. Chem.* **2004**, *47*, 3999.
- Kryger, G.; Silman, I.; Sussman, J. L. *Structure* **1999**, *7*, 297.
- Saxena, A.; Quian, N.; Kovach, I. M.; Kozikovski, A. P.; Pang, Y. P.; Vellom, D. C.; Radić, Z.; Quinn, D.; Taylor, P.; Doctor, B. P. *Protein Sci.* **1994**, *3*, 1770.
- Saxena, A.; Redman, A. M. G.; Jiang, X.; Lockridge, O.; Doctor, B. P. *Biochemistry* **1997**, *36*, 14642.
- (a) Boström, J. *J. Comput. Aided Mol. Des.* **2002**, *15*, 1137; (b) Boström, J.; Greenwood, J. R.; Gottfries, J. *J. Mol. Graph. Modell.* **2003**, *21*, 449. www.eyesopen.com.
- Halgren, T. A. *J. Comp. Chem.* **1999**, *20*, 720.
- Stewart, J. J. P. *J. Mol. Mod.* **2007**, *13*, 1173. MOPAC2007, Stewart Computational Chemistry, Colorado Springs, CO, USA, <http://OpenMOPAC.net>.
- Duran, A.; Martinez, G. C.; Pastor, M. J. *Chem. Inf. Model.* **2008**, *48*, 1813; Pentacle 1.0 prerelease, www.moldiscovery.com.
- Goodford, P. J. *J. Med. Chem.* **1985**, *28*, 849; GRID 22b; <http://www.moldiscovery.com>.
- Ermondi, G.; Anghilante, C.; Caron, G. *J. Mol. Graph. Modell.* **2006**, *25*, 296; BIOCUBE v1.0.0 <http://www.casmedchem.unito.it>.
- Guex, N.; Peitsch, M. C. *Electrophoresis* **1997**, *18*, 2714; <http://www.expasy.org/spdv>.
- Sanner, M. F. *J. Mol. Graph. Modell.* **1999**, *17*, 57; AUTODOCK Tools 1.5.4.
- Pedretti, A.; Villa, L.; Vistoli, G. *J. Comput. Aid. Mol. Des.* **2004**, *18*, 167; VegaZZ 2.3.1 <http://www.ddl.unimi.it>.